New Insights into Crustal Contributions to Large-volume Rhyolite Generation in the Mid-Tertiary Sierra Madre Occidental Province, Mexico, Revealed by U–Pb Geochronology

SCOTT E. BRYAN[1]*, LUCA FERRARI[2], PETER W. REINERS[1,†], CHARLOTTE M. ALLEN[3], CHIARA M. PETRONE[4], ALDO RAMOS-ROSIQUE[2,5] AND IAN H. CAMPBELL[3]

[1]DEPARTMENT OF GEOLOGY & GEOPHYSICS, YALE UNIVERSITY, PO BOX 208109, NEW HAVEN, CT 06520-8109, USA

[2]CENTRO DE GEOCIENCIAS, UNIVERSIDAD NACIONAL AUTÓNOMA DE MEXICO, CAMPUS JURIQUILLA, QUERETARO 76230, MEXICO

[3]RESEARCH SCHOOL OF EARTH SCIENCES, AUSTRALIAN NATIONAL UNIVERSITY, CANBERRA, A.C.T. 0200, AUSTRALIA

[4]C.N.R.–ISTITUTO GEOSCIENCE E GEORISORSE, U.O. FIRENZE, VIA G. LA PIRA 4, 50121 FIRENZE, ITALY

[5]CENTRE FOR EARTH AND ENVIRONMENTAL SCIENCE RESEARCH, KINGSTON UNIVERSITY, PENHRYN ROAD, KINGSTON UPON THAMES KT1 2EE, UK

Voluminous ($\geq 3{\cdot}9 \times 10^5\,km^3$), *prolonged* ($\sim$18 *Myr*) *explosive silicic volcanism makes the mid-Tertiary Sierra Madre Occidental province of Mexico one of the largest intact silicic volcanic provinces known. Previous models have proposed an assimilation–fractional crystallization origin for the rhyolites involving closed-system fractional crystallization from crustally contaminated andesitic parental magmas, with <20% crustal contributions. The lack of isotopic variation among the lower crustal xenoliths inferred to represent the crustal contaminants and coeval Sierra Madre Occidental rhyolite and basaltic andesite to andesite volcanic rocks has constrained interpretations for larger crustal contributions. Here, we use zircon age populations as probes to assess crustal involvement in Sierra Madre Occidental silicic magmatism. Laser ablation-inductively coupled plasma-mass spectrometry analyses of zircons from rhyolitic ignimbrites from the northeastern and southwestern sectors of the province yield U–Pb ages that show significant age discrepancies of 1–4 Myr compared with previously determined K/Ar and* $^{40}Ar/^{39}Ar$ *ages from the same ignimbrites; the age differences are greater than the errors attributable to analytical uncertainty. Zircon xenocrysts with new overgrowths in the Late Eocene to earliest Oligocene rhyolite ignimbrites from the northeastern sector provide direct evidence for some involvement of Proterozoic crustal materials, and, potentially more importantly, the derivation of zircon from Mesozoic and Eocene age, isotopically primitive, subduction-related igneous basement. The youngest rhyolitic ignimbrites from the southwestern sector show even stronger evidence for inheritance in the age spectra, but lack old*

*Corresponding author. Present address: Centre for Earth and Environmental Science Research, Kingston University, Penhryn Road, Kingston upon Thames KT1 2EE, UK. E-mail: s.bryan@kingston.ac.uk

†Present address: Department of Geosciences, University of Arizona, Gould-Simpson Building #77, 1040 E 4th Street, Tucson, AZ 85721, USA.

inherited zircon (i.e. Eocene or older). Instead, these Early Miocene ignimbrites are dominated by antecrystic zircons, representing >33 to ~100% of the dated population; most antecrysts range in age between ~20 and 32 Ma. A sub-population of the antecrystic zircons is chemically distinct in terms of their high U (>1000 ppm to 1·3 wt %) and heavy REE contents; these are not present in the Oligocene ignimbrites in the northeastern sector of the Sierra Madre Occidental. The combination of antecryst zircon U–Pb ages and chemistry suggests that much of the zircon in the youngest rhyolites was derived by remelting of partially molten to solidified igneous rocks formed during preceding phases of Sierra Madre Occidental volcanism. Strong Zr undersaturation, and estimations for very rapid dissolution rates of entrained zircons, preclude coeval mafic magmas being parental to the rhyolite magmas by a process of lower crustal assimilation followed by closed-system crystal fractionation as interpreted in previous studies of the Sierra Madre Occidental rhyolites. Mafic magmas were more probably important in providing a long-lived heat and material flux into the crust, resulting in the remelting and recycling of older crust and newly formed igneous materials related to Sierra Madre Occidental magmatism.

INTRODUCTION

Rhyolitic volcanoes (calderas) and granitic batholiths are the major manifestations of silicic magmatism, and are important igneous building blocks of continents. Rhyolitic volcanoes have the potential to produce enormous ($>10^2$–$10^4 km^3$), caldera-forming eruptions that pose widespread environmental hazards. The largest volume eruptions currently known from the geological record are silicic [e.g. the $>6340 km^3$ (dense rock equivalent) Springbok Quartz-Latite of Namibia, Ewart *et al.*, 1998].

Silicic magmatism on the continents can be extensive ($>10^5 km^2$), with substantial cumulative volumes (10^4 to $>10^6 km^3$) and relatively long-lived to pulsatory (10–40 Myr; Table 1). The largest belts of silicic igneous activity have been referred to as Silicic Large Igneous Provinces (SLIPs, Bryan *et al.*, 2002; Bryan, 2007; Bryan & Ernst, 2007). Such large-scale silicic magmatism must ultimately derive its thermal energy from the mantle (e.g. Hildreth, 1981). A fundamental question then is whether the large-volume silicic magmatism of SLIPs represents new additions to the continents of magmas derived from the mantle, or whether it mostly reflects recycling of continental crust through partial melting caused by the addition of enthalpy supplied by mafic magmas (e.g. see Dufek & Bergantz, 2005).

Whole-rock geochemical and isotopic studies have previously been used to constrain the proportions of crust and mantle additions to rhyolite magmatism, from which new episodes of continental growth may be identified (e.g. Ruiz *et al.*, 1988*a*; Farmer, 1992; Perry *et al.*, 1993). However, conclusions from these types of studies are often ambiguous because of a combined lack of information on the age, composition and isotopic characteristics of local basement rocks, and the potential lack of isotopic distinctions between pre-existing crustal materials and underlying upper mantle. The distinction is further blurred in cases where the initial $^{87}Sr/^{86}Sr$ ratios and Pb isotopic compositions of some rhyolites are unradiogenic and similar to those of the associated basalts (e.g. the Karoo and Deccan flood basalt provinces), indicating derivation from a primitive mafic source. This has led to interpretations of rhyolite petrogenesis by partial melting of newly underplated basaltic magma with superimposed fractional crystallization (Cleverly *et al.*, 1984; Lightfoot *et al.*, 1987). Constraining the age and composition of the continental crust involved in rhyolite magmatism is, ítherefore, an

Table 1: Catalogue of large silicic igneous provinces ordered in terms of minimum estimated extrusive volumes

Province	Age (Ma)	Volume (km³)	Dimensions (km)	Magma flux (km³/kyr)	References
Whitsunday (Eastern Australia)	~132–95	$>2·2 \times 10^6$	$>2500 \times 200$	>55	Bryan *et al.* (1997, 2000)
Kennedy–Connors–Auburn (NE Australia)	~320–280	$>5 \times 10^5$	$>1900 \times 300$	>12·5	Bain & Draper (1997); Bryan *et al.* (2003)
Sierra Madre Occidental (Mexico)	~38–20	$>3·9 \times 10^5$	$>2000 \times 200$–500	>22	Ferrari *et al.* (2002); Aguirre-Díaz & Labarthe-Hernandez (2003)
Chon Aike (South America–Antarctica)	188–153	$>2·3 \times 10^5$	$>3000 \times 1000$	>7·1	Pankhurst *et al.* (1998, 2000)
Altiplano–Puna (central Andes)	~10–3	$>3 \times 10^4$	$~300 \times 200$	>4·3	De Silva (1989*a*, 1989*b*)
Taupo Volcanic Zone (New Zealand)	1·6–0	$~2 \times 10^4$	300×60	~9·4–13	Houghton *et al.* (1995); Wilson *et al.* (1995)

All provinces are dominated by rhyolitic igneous compositions and ignimbrite. Magma flux rate is averaged eruptive flux, based on known extrusive volumes for the provinces.
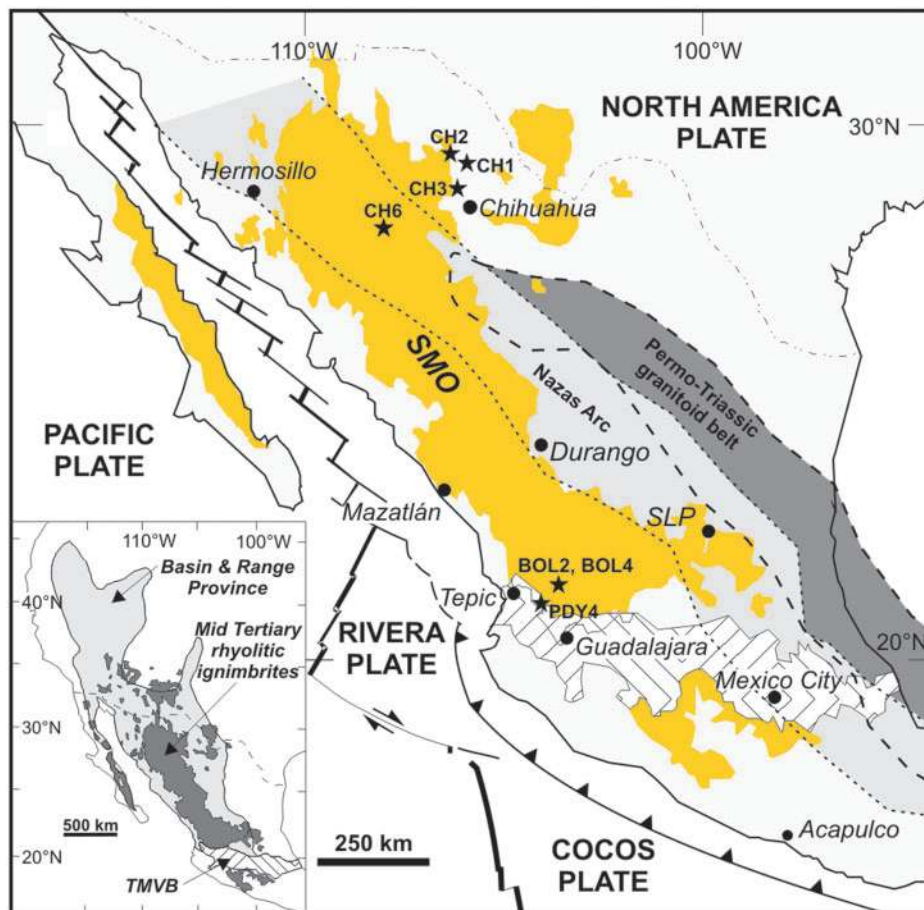
Fig. 1. Map of Mexico showing the present-day configuration of plates, location of the Sierra Madre Occidental (SMO) and distribution of Oligocene to Early Miocene, mostly silicic volcanic rocks. The cross-hatched area is the Trans-Mexican Volcanic Belt (TMVB), the current location of supra-subduction zone volcanism. The extent of the Early–Middle Jurassic subduction-related volcanic arc is in light grey shading and bounded by dotted lines (Sedlock *et al.*, 1993; Jones *et al.*, 1995; Nazas arc of Bartolini, 1998, and Dickinson & Lawton, 2001). The Permo-Triassic granitoid belt is a darker grey shade bounded by dashed lines (Torres *et al.*, 1999). Stars denote ignimbrite sample locations for which U/Pb zircon age dates have been obtained in this study. SLP, San Luis Potosi. Inset shows outcrops of Middle Tertiary rhyolite ignimbrites in Mexico and SW USA and the extent of the Basin and Range Province, both of which overlap in space and time. Modified from Ferrari *et al.* (2002) and Aguirre-Díaz & Labarthe-Hernandez (2003).

essential first step to quantify the proportion of mantle-derived melts contributing to silicic magmas and thus to the crust.

The mid-Tertiary Sierra Madre Occidental (SMO) volcanic province of Mexico (Fig. 1) provides an example of the debate over the relative contributions of mantle and crustal melts to the huge volumes of rhyolitic ignimbrite, and consequently, how much new continental crustal growth has occurred. After initial studies suggesting that the large volumes of silicic volcanic rocks formed entirely by fractional crystallization from basaltic parental magmas (e.g. Cameron *et al.*, 1980*a*; Lanphere *et al.*, 1980), most current models indicate that the SMO rhyolites are end-products of crystal fractionation from andesitic parental magmas that formed as a result of limited (<20%) crustal assimilation by mantle-derived basaltic magmas

(AFC, e.g. Wark, 1991; Smith *et al.*, 1996). In contrast, other workers have suggested that crustal contributions to the rhyolite magmas are much larger (up to 70%, Albrecht & Goldstein, 2000), and that based on isotopic constraints from crustal xenoliths, the rhyolites could potentially be derived entirely by crustal melting (e.g. Ruiz *et al.*, 1988*a*, 1990). In all of the studies, estimates of the proportions of mantle and crustal components in the rhyolite magmas are strongly dependent on the assumed isotopic compositions of the underlying mantle and crust (Cameron & Robinson, 1990; Wark, 1991; Smith *et al.*, 1996).

In this study, we use zircon U–Pb ages and trace element compositions from ignimbrite eruptive units of the SMO as tools to identify crustal source materials involved in the petrogenesis of the magmas. In particular, we focus on zircon xenocrysts, which are interpreted as

the surviving remnants of older crustal materials, to constrain the ages and types of crustal materials involved in rhyolite petrogenesis. Magmatic overgrowths on inherited zircon cores indicate that the cores were formed prior to residence in the magma chamber, as opposed to being accidental grains incorporated into the magma during eruption (Miller *et al.*, 2003). Studying zircon inheritance in rhyolitic volcanic rocks has several advantages as a crustal probe: (1) zircon is far more abundant in the rhyolites than in the small xenoliths that are commonly used as samples of the crust; (2) rhyolites potentially sample large volumes of crust via melting or assimilation in MASH zones (Hildreth & Moorbath, 1988), and, by virtue of the extent of the volcanic belt ($>10^5$ km^2), provide a greater sampling of lower crustal materials; and (3) the rhyolites can provide a 'real-time' record of changes in the magma source regions in the crust. Dating and chemical analysis by Excimer laser ablation-inductively coupled plasma-mass spectrometry in combination with cathodoluminescence studies are used to assess inherited [antecrystic to xenocrystic, following the terminology of Charlier *et al.* (2004)] components within zircon crystal populations. The main conclusions derived from our zircon data are that: (1) young (Eocene to Early Miocene), isotopically primitive crustal materials were important crustal source components of the rhyolites; (2) the inherited zircons provide a more direct record of the age and type of crustal materials involved in rhyolite petrogenesis; these ages and therefore types of crustal materials can potentially be very different from those of the crustal xenoliths upon which petrogenetic studies have been based; and (3) binary models of mixing–AFC processes for SMO rhyolite petrogenesis are oversimplified, as contributions from multiple crustal sources of different ages (Proterozoic, Mesozoic, Tertiary), and chemical and isotopic composition, are likely to have been involved, and have changed through time.

SIERRA MADRE OCCIDENTAL

The mid-Tertiary SMO (Fig. 1) is the largest silicic igneous province in North America (McDowell & Keizer, 1977; McDowell & Clabaugh, 1979; Ward, 1995). It is 200–500 km wide and extends for more than 2000 km south from the US–Mexico border to its intersection with the Trans-Mexican Volcanic Belt. At least 3.9×10^5 km^3 of dominantly rhyolitic ignimbrites were erupted from Late Eocene to Early Miocene times, covering an enormous area of Mexico to an average thickness of 1 km (e.g. McDowell & Clabaugh, 1979; Ferrari *et al.*, 2002, 2007; Aguirre-Díaz & Labarthe-Hernandez, 2003). Numerous, mostly K/Ar, geochronological studies of the SMO indicate that most of the rhyolites were erupted between ∼38 and 20 Ma (McDowell & Keizer, 1977; McDowell & Clabaugh, 1979; McDowell & Mauger, 1994;

Nieto-Samaniego *et al.*, 1999, and references therein; Ferrari *et al.*, 2002, 2007). Some ignimbrites exposed in the eastern and western parts of the SMO proper have older ages extending back to 45–55 Ma (e.g. Aguirre-Díaz & McDowell, 1991; McDowell & Mauger, 1994; Gans, 1997), and McDowell & McIntosh (2007) have recently identified an Eocene ignimbrite pulse across the northern SMO at 44.1–45.4 Ma. For the central and southern SMO, available age data suggest two periods of ignimbrite activity at ∼32–28 Ma and ∼24–20 Ma (Ferrari *et al.*, 2002, 2007).

Most SMO ignimbrites contain a phenocryst assemblage of plagioclase, quartz, and Fe–Ti oxides; alkali feldspar is uncommon, and the ferromagnesian phases are dominated by pyroxene, biotite and/or hornblende (e.g. Swanson *et al.*, 1978, 2006; Cameron *et al.*, 1980*a*; Wark, 1991). Although the ignimbrite phenocryst assemblages resemble those of 'orogenic' silicic volcanic rocks, they tend to contain less hornblende and biotite; ignimbrites in the northern SMO are predominantly pyroxene rhyolites (Cameron *et al.*, 1980*b*). The ignimbrites display considerable variation in crystal content, with crystal-poor (<10%) and crystal-rich (up to 50%) types present (e.g. Swanson *et al.*, 2006). The crystal-rich ignimbrites may have an origin similar to that proposed for the coeval crystal-rich 'monotonous intermediates' of the Great Basin and San Juan volcanic field erupted along strike to the north (Hildreth, 1981; Bachmann *et al.*, 2002; Maughan *et al.*, 2002; Bachmann & Bergantz, 2003).

Like the SLIPs in Table 1, the SMO is dominated by rhyolite, but with mafic to intermediate rocks present that result in a spectrum of compositions between ∼49 and 78 wt % SiO$_2$ (e.g. Cameron *et al.*, 1980*a*; Wark, 1991; Albrecht & Goldstein, 2000; Bryan, 2007). However, igneous rocks dated between 34 and 20 Ma are compositionally bimodal with volumetrically dominant silicic (∼66–78 wt % SiO$_2$) and volumetrically minor mafic (50–58 wt % SiO$_2$) magma types; intermediate compositions (∼62–66 wt % SiO$_2$) are rare (Bryan, 2007; Ferrari *et al.*, 2007). Ignimbrite compositions are dominantly in the range 68–75 wt % SiO$_2$ whereas interbedded rhyolitic lavas extend to high-silica rhyolite compositions (>75 wt % SiO$_2$; Cameron *et al.*, 1980*a*). Basaltic rocks erupted across the SMO between 34 and 20 Ma show some compositional variation as evidenced in their minor and trace element contents, reflecting the presence of low-Ti ($\leq$1 wt %) and high-Ti (>2 wt %) basaltic magma types (Bryan, 2007). The volcanic rocks have medium- to high-K calc-alkaline compositions and initial ^{87}Sr/^{86}Sr ratios ranging from 0.7044 to ∼0.710 that show no systematic variation with rock composition (Lanphere *et al.*, 1980; Wark, 1991; Albrecht & Goldstein, 2000). Both the rhyolites and basalts have geochemical signatures transitional between within-plate and convergent margin fields on trace element discrimination diagrams (Bryan, 2007).

The continent-margin position, calc-alkaline affinity, isotopic characteristics and association with continued subduction beneath western North America have led many workers to consider the SMO as a subduction-related volcanic arc (e.g. McDowell & Clabaugh, 1979; Cameron *et al.*, 1980*b*; Wark *et al.*, 1990; Wark, 1991). However, the overwhelming silicic composition, the eruptive scale, volume and output rate (Table 1), and the ignimbrite-dominated character of the erupted products sourced from multiple calderas and fissures (Swanson & McDowell, 1984; Aguirre-Díaz & Labarthe-Hernandez, 2003; Swanson *et al.*, 2006) are inconsistent with modern expressions of supra-subduction zone volcanism; nor are narrow, silicic-magma dominated continental arc- to back-arc rifts like the Taupo Volcanic Zone (Cole, 1990; Wilson *et al.*, 1995; Parson & Wright, 1996) appropriate analogues. This magmatism occurred at a time when andesitic (supra-subduction zone) magmatism was rare, and increased divergence of the Pacific and North American plates resulted in extension of the continental margin (Ward, 1995). SMO ignimbrite activity was concurrent with widespread, predominantly explosive silicic volcanism (the 'ignimbrite flare-up') in the Basin & Range Province of the western USA (Fig. 1) where $>10^5 km^3$ of dacitic to rhyolitic ignimbrites were emplaced between ~35 and 20 Ma (Lipman *et al.*, 1972; Gans *et al.*, 1989; Best & Christiansen, 1991; Johnson, 1991). The SMO represents a large region of the North American Cordillera that lacked rapid syn-volcanic extension, in contrast to other Cordilleran regions during this period (Gans & Bohrson, 1997). It shares many characteristics with the rift-related Mesozoic SLIPs of Table 1 (Bryan, 2007) and may be related to continental extension that eventually led to the opening of the Gulf of California in the Late Miocene.

Basement and crustal structure to the SMO

The regional geology of the basement rocks and crustal structure beneath the SMO has recently been reviewed by Centeno-Garcia *et al.* (2007) and Ferrari *et al.* (2007), and for the northern SMO by Housh & McDowell (2007). SMO magmas were emplaced through crust that varies from Laurentian basement contiguous with the North American Craton in the north to Mesozoic age subduction complexes and volcanogenic terranes beneath the core of the SMO and to the south (Fig. 2). However, the majority of surface exposures of basement units within the SMO are of Cretaceous to Eocene age. Old North American basement is thought to underlie at least the northern SMO, as evidenced by Precambrian rocks cropping out ~40 km north of Chihuahua City (Blount *et al.* 1988; Blount, 1993), which have clearly modified the isotopic composition of the Cenozoic volcanic rocks in that region. Zircon inheritance in Cretaceous to Eocene rocks confirms the existence of Precambrian basement in east–central Sonora and central Chihuahua (McDowell & Mauger,

1994; McDowell *et al.*, 2001), whereas lower crustal xenoliths in the Neogene–Quaternary alkali basalts at El Potrerillo and La Olivina (Ruiz *et al.*, 1988*b*; Cameron *et al.*, 1992) indicate the extension of Proterozoic crystalline rocks to beneath northeastern and southeastern Chihuahua. Recent isotopic studies of Laramide granitic rocks from northwestern Mexico suggest that the Proterozoic crustal boundary may be located further to the south, near the Sonora–Sinaloa–Chihuahua state borders (Valencia-Moreno *et al.*, 2001, 2003). Available U–Pb zircon ages for Precambrian rocks at the southern margin of the North American craton in western Texas and northern Chihuahua, comprising granitic plutons, gneiss and schist and the metamorphosed clastic and volcanic rocks of the Pinal schist, range between ~1·35 and 1·1 Ga, and up to 1·7–1·8 Ga in the NW of Sonora state (Mexico) along the northwestern edge of the SMO (James & Henry, 1993; McDowell *et al.*, 1999, and references therein; Housh & McDowell, 2007).

The existence of Proterozoic crust beneath the central and southern SMO is more controversial; here the basement is generally considered to comprise accreted sections of volcanosedimentary rocks built by Mesozoic island arc magmatism (Guerrero composite terrane; Campa & Coney, 1983; Dickinson & Lawton, 2001). However, incorporated within the Guerrero composite terrane are metamorphosed volcanosedimentary rocks as old as Ordovician, as well as more widespread Permo-Triassic metasedimentary rocks with a North American craton provenance, implying proximity to the continent, and sediment accumulation along the palaeocontinental shelf–slope of western North America (Centeno-Garcia *et al.*, 2007). The likely presence of Palaeozoic and Precambrian crustal materials beneath the Guerrero terrane in southern Mexico is also indicated from xenolith studies (e.g. Elías-Herrera & Ortega-Gutiérrez, 1997; Aguirre-Díaz *et al.*, 2002), inherited zircons and the Nd model ages of the igneous rocks (e.g. Schaaf *et al.*, 2003; Levresse *et al.*, 2004).

The Proterozoic crystalline rocks of northern and northwestern Mexico are covered by Neoproterozoic to Palaeozoic marine sedimentary rocks deposited along the margin of the North American craton. The Neoproterozoic and Palaeozoic rocks clearly continue beneath the Tertiary volcanic rocks of the SMO in eastern Sonora, with the southernmost exposures of Neoproterozoic to Palaeozoic rocks occurring in northern Durango and northern Sinaloa along the western edge of the SMO, where muscovite schists and metamorphosed volcanosedimentary rocks are exposed (Ferrari *et al.*, 2007).

Mesozoic rocks are well exposed along the western side of the SMO in Sonora and Sinaloa, comprising clastic continental and marine sedimentary rocks of Late Triassic–Early Jurassic age (Barranca Group, Stewart &
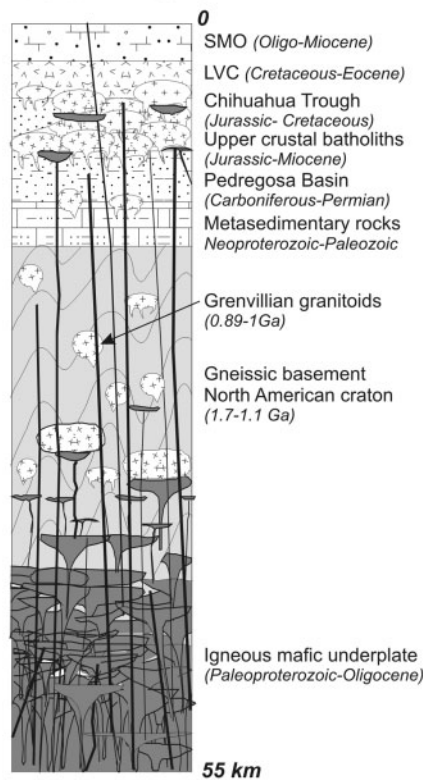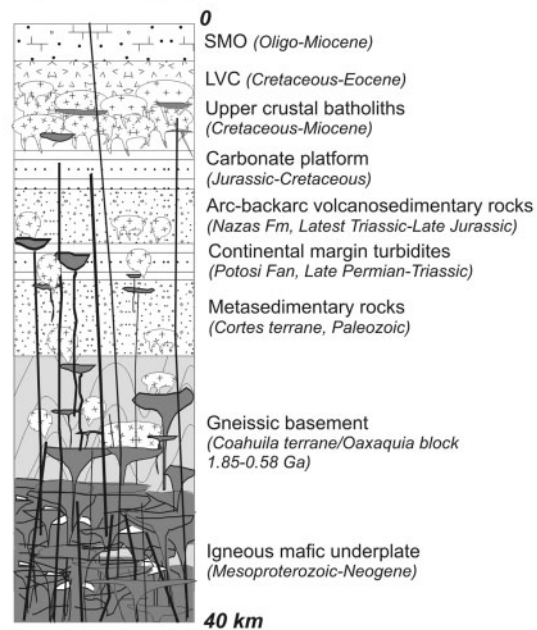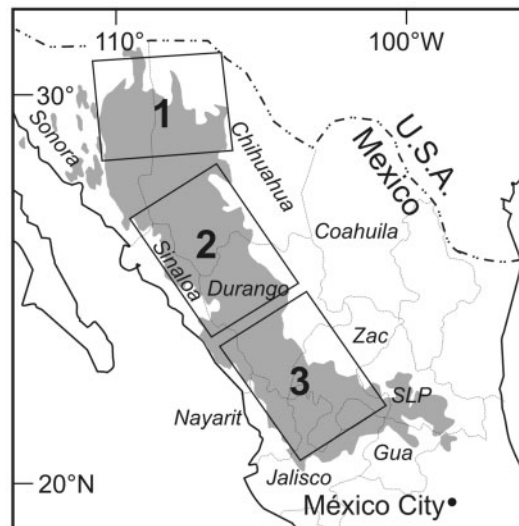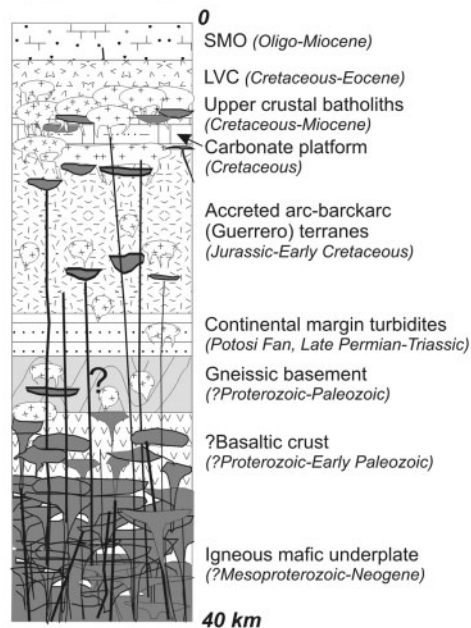
Fig. 2. Schematic crustal sections showing the inferred architecture, age and composition of the crust beneath the northern, central and southern SMO (see inset), based on Centeno-Garcia *et al.* (2007), Ferrari *et al.* (2007) and Housh & McDowell (2007), and references therein. The thickness of each crustal section is based on Bonner & Herrin (1999) for the northern SMO, and Couch *et al.* (1991) for the central and southern SMO. The thicknesses of the component crustal units are not to scale. States mentioned in text are shown in the inset map. LVC, Lower Volcanic Complex; Zac, Zacatecas; Gua, Guanajuato; SLP, San Luis Potosi.

Roldán-Quintana, 1991; Valencia-Moreno *et al.*, 1999; Antimonio Group, González-León, 1997). The Antimonio Group and associated plutonic rocks have been interpreted as products of a Jurassic subduction-related continental arc. Igneous rocks of similar ages from the eastern margin of the SMO in southern Chihuahua and northern Durango have been interpreted as an extension of this Triassic–Jurassic arc, but displaced to the east by the Mojave–Sonora megashear (Grajales-Nishimura *et al.*, 1992). A solitary Late Triassic pluton exposed in northwestern Sonora provides the basis for suggesting that subduction-related magmatic activity through northwestern Mexico was relatively continuous from ~220 to 140 Ma (e.g. Anderson & Silver, 1979; Damon *et al.*, 1981; Stewart, 1988). However, the lack of Triassic igneous-derived detrital zircons in the turbidites of the Potosi Fan constructed along the Mexican continental margin suggests a lack of Late Triassic continental arc volcanism in Mexico (Centeno-Garcia *et al.*, 2007).

Unconformably overlying the Jurassic sequences are extensive, predominantly marine volcanosedimentary rocks and limestones of Late Jurassic to Early Cretaceous age that extend from the western to eastern margins of the SMO. These include the Alisitos Formation exposed mainly in the northern part of Baja California, which represents the accreted remnants of a rifted oceanic arc terrane (e.g. Busby *et al.*, 1998). Small exposures of pre-Cenozoic slate, greywacke and limestone suggest a continuation of Late Jurassic and Early Cretaceous rocks beneath the southern SMO (Ferrari *et al.*, 2007).

Much of the Oligocene ignimbrite pile of the SMO directly overlies Late Cretaceous–Paleocene igneous rocks that were emplaced as part of Cordilleran magmatic activity temporally associated with Laramide deformation in the western USA and Canada. Significant volumes of plutonic and volcanic rocks were produced during this event, and have been collectively grouped into the Lower Volcanic Complex by McDowell & Keizer (1977). The Lower Volcanic Complex is considerably wider in Sonora than its extension to the south into Sinaloa, which may reflect the greater effect of Neogene Basin and Range extension to the north (Damon *et al.*, 1983). Although largely concealed by the SMO ignimbrites, particularly in the southern SMO, Lower Volcanic Complex rocks are indicated to extend further east of the SMO into Chihuahua (see Mauger, 1981, 1983; McDowell & Mauger, 1994) and Zacatecas (Ferrari *et al.*, 2007; Solé *et al.*, 2007).

Cretaceous–Paleocene batholiths probably underlie a large part of the SMO (Fig. 2). All known intrusive rocks are calc-alkaline in composition, and vary from diorite to granite, but granodioritic plutons are by far the dominant composition. The ages of the batholithic rocks in Sonora range between 91 and 43 Ma, and become progressively younger to the east (Damon *et al.*, 1983), whereas the volcanic rocks of the complex in the east–central part of Sonora were emplaced between 90 and 60 Ma (McDowell *et al.*, 2001). Granitic rocks of the Sinaloa Batholith in the central SMO have U–Pb and K–Ar ages between 101 and 46 Ma (Henry *et al.*, 2003). The Lower Volcanic Complex of McDowell & Clabaugh (1979) also included older rocks (~120–85 Ma) of the Peninsular Ranges Batholith of Baja California and its extension into Sinaloa.

Eocene magmatic activity has generally been included as part of the Lower Volcanic Complex; however, recent studies (e.g. Aguirre-Díaz & McDowell, 1991) have documented the considerable space–time extent of this volcanic event, suggesting it was a distinct episode in the magmatic evolution of western Mexico (Ferrari *et al.*, 2007). Eocene (~53–40 Ma) andesitic to rhyolitic magmatism is speculated to have formed a similarly extensive, broad belt to the overlying Oligocene SMO. Some exposed sections of Eocene rocks have substantial thicknesses (>1 km), comprising andesitic to rhyolitic lavas and rhyolitic ignimbrites, in places cross-cut by minor subvolcanic intrusions of diorite to granodiorite. In the northern SMO (Chihuahua), Eocene volcanic activity began at 46 Ma after a period of scarce and intermittent magmatism, and continued, almost without interruption, until 27·5 Ma (Ferrari *et al.*, 2007). In the central and southern SMO, Eocene volcanism began at ~48 Ma and likewise continued until the onset of the first ignimbrite 'flare-up' at 33–32 Ma.

In summary, crustal basement ages beneath the SMO increase from south to north with accreted Mesozoic, subduction-related igneous and sedimentary rocks dominating the crustal profile beneath the southern SMO, a Grenvillian age gneissic terrane [Oaxaquia microcontinent of Ortega-Gutiérrez *et al.* (1994) and Coahuila block of Coney & Campa (1987)] and early Palaeozoic sedimentary rocks beneath the central SMO, and Palaeoproterozoic to Mesoproterozoic age crust of the North American craton beneath the northernmost SMO (Fig. 2). Previous geochemical studies of the SMO rhyolites have identified spatial variations in trace element (e.g. Nb, Zr, Th, Rb) and isotopic compositions that correlate with the age and composition of the basement rocks (Albrecht & Goldstein, 2000; see also Cameron *et al.*, 1980*a*). However, superimposed on this crustal basement architecture has been the intrusion and underplating of substantial volumes of igneous material particularly during the Mesozoic and Cenozoic, such that: (1) Cretaceous to Palaeogene batholithic and volcanic rocks probably represent the overwhelming volume of upper crustal rocks; and (2) a significant proportion of Mesozoic–Early Tertiary age igneous intrusions may have resided in the lower crust beneath the SMO, immediately prior to the

Table 2: List of samples analysed in this study

Sample	Location	Geographical location	Lithology
Group 1, Northeastern sector			
CH1*	0372669 mE, 3268158 mN	Road to Ojo de Laguna microwave station	Upper unit of crystal-rich, oligoclase–sanidine–augite-phyricrhyolitic rheomorphic ignimbrite
CH2	0335862 mE, 3307387 mN	Sierra Los Arados	Welded quartz–sanidine-phyric rhyolite ignimbrite
CH3	0365043 mE, 3217789 mN	North of Bellavista Canyon	Welded plagioclase–quartz-phyric rhyolitic ignimbrite
CH6[†]	0199140 mE, 3129943 mN	Roadcut between Tomochíc and Basaseachic	Welded crystal-rich, quartz–plagioclase–sanidine–biotite–hornblende-phyric ignimbrite
Group 2, Southwestern sector			
BOL2	626837 mE, 2410312 mN	Rio Carboneras, Bolaños Graben	Welded plagioclase–quartz–hornblende-phyric rhyolite ignimbrite
BOL4[‡]	628318 mE, 2414535 mN	Cerro Aguila, Bolaños Graben	Nonwelded crystal-poor, sanidine–plagioclase–quartz–biotite-phyric rhyolitic ignimbrite
PDY4	595327 mE, 2337189 mN	Rio Santiago, near Paso de la Yesca	Welded crystal-rich, plagioclase–quartz–biotite-phyric rhyolite ignimbrite

UTM grid coordinates are from the NAD83 map datum, zone 13.
*Gallego Rhyolite of Keller *et al.* (1982).
[†]Vista Tuff of Swanson & McDowell (1985) and Wark *et al.* (1990).
[‡]Alacrán ignimbrite of Scheubel *et al.* (1988) and Aguirre-Díaz & Labarthe-Hernandez (2003).

Oligocene ignimbrite 'flare-up'. Consequently, along the length of the SMO, the age of the lower crust may be significantly younger than the age of the exposed basement (see also Klemperer, 1989).

SAMPLES AND ANALYTICAL METHODS

Two groups of samples were collected (Table 2): one group from the northeastern sector, in the central part of the state of Chihuahua, where a considerable body of previous work has been undertaken (e.g. Keller *et al.*, 1982; Swanson & McDowell, 1985; Wark *et al.*, 1990; Wark, 1991; McDowell & Mauger, 1994; McDowell *et al.*, 1999); and a second group from the southwestern sector of the SMO (Fig. 1) in the Bolaños Graben (see Ferrari *et al.*, 2002), and near the confluence of the Bolaños and Santiago rivers, ~80 km SW of the city of Tepic (see Ferrari *et al.*, 2000). Group 1 samples are from sections that contain some of the oldest dated ignimbrites associated with SMO activity, whereas Group 2 samples are from the youngest (<24 Ma) sections of the SMO volcanic pile, based on previous K/Ar dating (see Ferrari *et al.*, 1999, 2002). Between 2 and 5 kg of sample was collected and processed using standard crushing and mineral separation techniques. Additional information on analytical techniques is given in the Appendix.

U–Pb ELA-ICP-MS analysis

U–Pb isotopic compositions of zircons were analysed at the Australian National University, Canberra, using Excimer laser ablation-inductively coupled plasma-mass spectrometry (ELA-ICP-MS). The reader is referred to Bryan *et al.* (2004), Harris *et al.* (2004) and Allen & Barnes (2006) for further details on the zircon analytical technique and procedures, which are essentially identical in this study. The purpose in all of these studies was to date the rock sample, but also to determine the ages of inheritance. The ELA-ICP-MS method for dating zircons has been developed to the point where the precision and accuracy of ELA-ICP-MS dates from the Australian National University, for young felsic rocks, are comparable with sensitive high-resolution ion microprobe (SHRIMP) ages, as well as being comparable with those ages determined by the K/Ar and $^{40}Ar/^{39}Ar$ methods down to ages of 3 Ma (Rohrlach, 2002; Black *et al.*, 2004; Harris *et al.*, 2004). Because zircon dating by this method is rapid, and throughput high, this method is suited to this type of study, where the emphasis is on finding and dating xenocrysts. Furthermore, if a sample has several distinct populations of xenocrystic zircons, then statistical methods can be applied to a large ELA-ICP-MS database to resolve and date the various populations.

Zircons in polished epoxy mounts (BOL2, BOL4, PDY4) or whole grains secured to a glass slide with double-sided tape (CH1-CH6) were ablated with a Lambda Physik LPX 120I ArF Excimer laser (193 nm wavelength)

Table 3: Precision of laser-ablation ICP-MS analyses with reference to NIST610 glass and 521 zircon standard materials

Date of analytical run	SD of $^{206}Pb/^{238}U$ on NIST610 averages	SD of $^{207}/^{206}Pb$ on NIST610 averages	*n/N*	521 zircon age weighted average (Ma)	2SE	MSWD	*n/N*	FCT zircon weighted average (Ma)	2SE	MSWD
27/04/04	0·69	0·29					9/12	27·98	0·67	2·58
02/12/04	1·77	0·25	12/12	42·33	0·48	1·30				
06/04/05	1·97	0·57	12/12	43·00	0·50	1·18				
02/07/05	0·4	0·38	8/8	42·31	0·24	0·91				
07/07/05	1·06	0·1								

The accepted ICP-MS age for 521 is $42·2 \pm 0·2$ Ma (Ballard *et al.*, 2001), and the concordia age for FCT zircons (including systematic decay constant errors and uncertainty in Pb/U tracer calibration) is $28·476 \pm 0·064$ Ma (Schmitz & Bowring, 2001).

connected to an Agilent 7500S quadrupole ICP-MS system. The laser settings and ICP instrument set-up are generally as reported by Eggins & Shelley (2002). Ablation hole diameters and depths were ~30 and ~20 μm, respectively. Masses used in geochronology (^{206}Pb, ^{207}Pb, ^{208}Pb, ^{232}Th, ^{235}U, ^{238}U) were each analysed for 0·04 s, and fractionation factors for ratios of these elements (except $^{232}Th/^{238}U$) were calculated from multiple ablations of the Temora2 zircon standard. Other elements of geochemical interest [^{29}Si, ^{31}P, ^{89}Y or ^{91}Zr, ^{177}Hf, and seven rare earth elements (REE)] were each collected for 0·01 s and fractionation factors for these elements ratioed to ^{29}Si, and $^{232}Th/^{238}U$ values were determined from NIST610. Data were collected in peak jumping mode with a mass sweep time of 0·384 s. A background (laser off signal) was collected for about 20 s at the beginning of each analysis, then a laser-on signal was collected for 35 s with a segment of surface ablation, and signal stabilization discarded (5 s).

Standard materials and groups of 10 unknowns were analysed in a round-robin fashion so that the averages of the standard over that day's analytical session were applicable. It shoule be noted that fractionation factors from the standards are calculated for each mass sweep, and are applied to the appropriate mass sweep of the laser-on signal in the unknown. The reproducibility of the ELA-ICP-MS technique was monitored by repeat analysis of natural zircon standards from the Los Picos porphyry from the Fortuna Complex, Chile (Ballard *et al.*, 2001), and the Fish Canyon Tuff, which have mid-Tertiary ages that are appropriate to the unknown SMO samples (Table 3). When uncertainties are properly quantified and applied to populations known to be of a single age, then MSWD values should converge at unity, as for the monitor standards. The uncertainty on the weighted mean age for the spectrum from single analyses includes an uncertainty term for measurement of the

Temora2 added in quadrature to the standard error in the measurement of the ratio for the unknown. Typically, uncertainty in $^{206}Pb/^{238}U$ expressed as standard deviation for tens of measurements of Temora is 1–1·5%. Thus, definition of a single age population is monitored by MSWD values.

Common Pb contents of zircons were not directly measured because systemic Hg isobarically interferes on mass 204, and the magnitude of background Hg is about 50 times that of total Pb. Estimation and correction for common Pb used a 208-based approach assuming a (Cumming & Richards, 1975) common Pb composition for the calculated age of that zircon. The percentage of common ^{206}Pb using the ^{208}Pb correction is generally less than 5% of the total ^{206}Pb (see the Electronic Appendix). The Cenozoic and Mesozoic ages reported here are based on $^{206}Pb/^{238}U$ ratios corrected for common Pb using a $^{208}Pb/^{232}Th$ basis. Uncertainties on ages of single grains are reported as 1σ, and on populations as 2σ. The complete U–Pb zircon geochronological dataset for samples is given in the Electronic Appendix, which may be downloaded from http://www.petrology.oxfordjournals.org; the results are presented in Figs 3 and 4.

Data were excluded from population age calculations on the basis of four criteria: (1) where inclusions were encountered in part of the analyses as identified, for instance, by anomalously high La or P (i.e. >500 ppm) suggesting intersection of an apatite inclusion; (2) if the measured uncertainty in the $^{206}Pb/^{238}U$ ratio used for dating grains <1000 Ma exceeded twice that expected from counting statistics; (3) lack of concordancy where concordancy is defined as when the 208 common Pb-corrected $^{206}Pb/^{238}U$ and $^{207}Pb/^{235}U$ ages (including uncertainty) agree within 3% (~1·5 Ma; Fig. 3); (4) by identifying outliers (e.g. caused by 'subtle' inheritance or Pb loss) through statistical analysis, probability plots (Figs 3 and 4), and composition (see the Electronic Appendix).
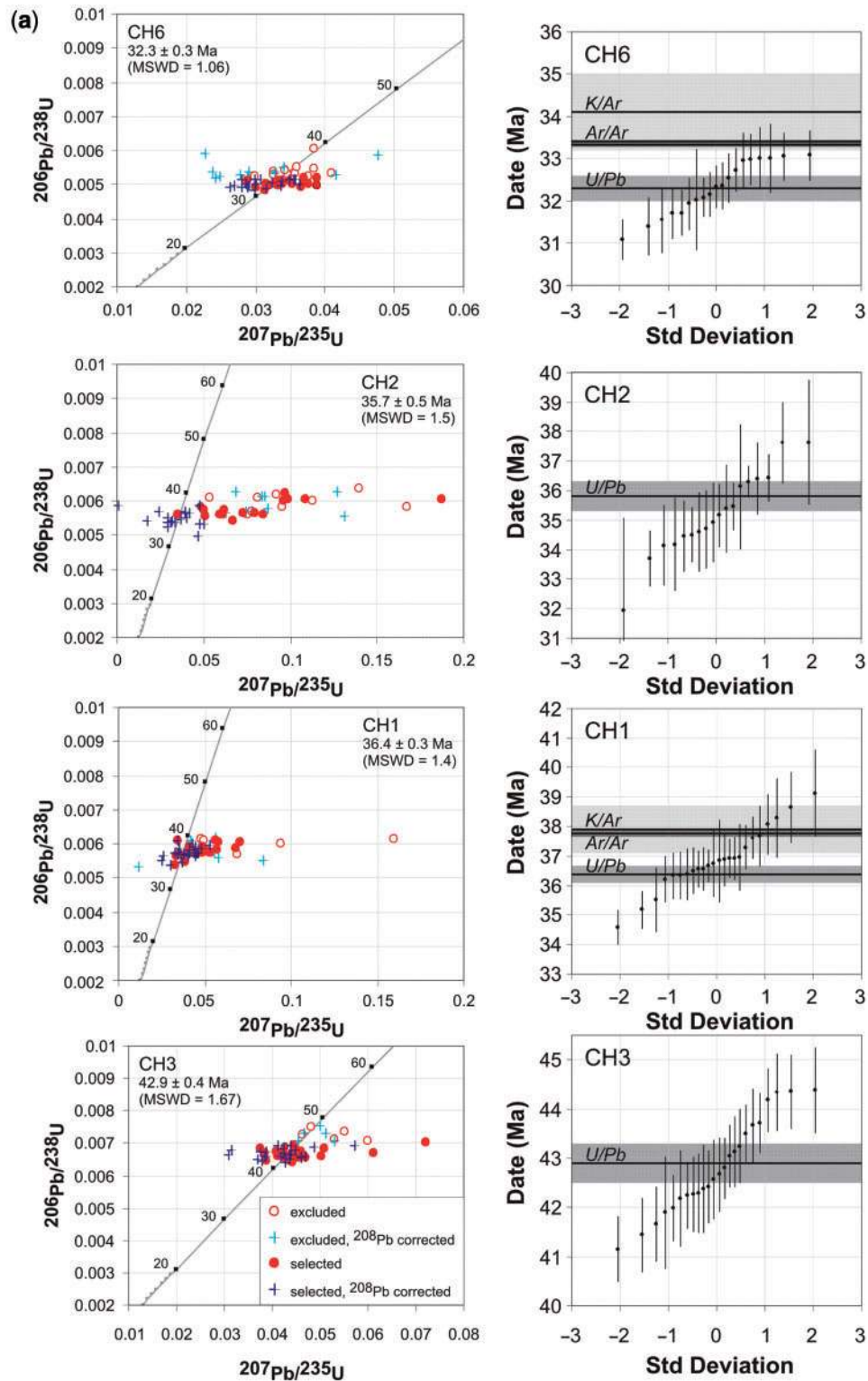
Fig. 3. Summary of ELA-ICP-MS analyses of igneous zircons from SMO rhyolite ignimbrites; sample abbreviations and information are given in Table 2. Concordia and probability plots are arranged in stratigraphic order for (a) Group 1 ignimbrites, northern SMO and (b) Group 2 ignimbrites, southern SMO. Concordia are shown with 10 Myr intervals on the concordia plots; ●, data used for the final age calculation; ○, omitted data, and both datasets are [208]Pb corrected. On the probability plots, the calculated weighted mean U–Pb age and available eruption age constraints from [40]Ar/[39]Ar and K/Ar dates with shaded error envelopes are shown for each sample. Error bars on the standard deviation plots are 1σ.
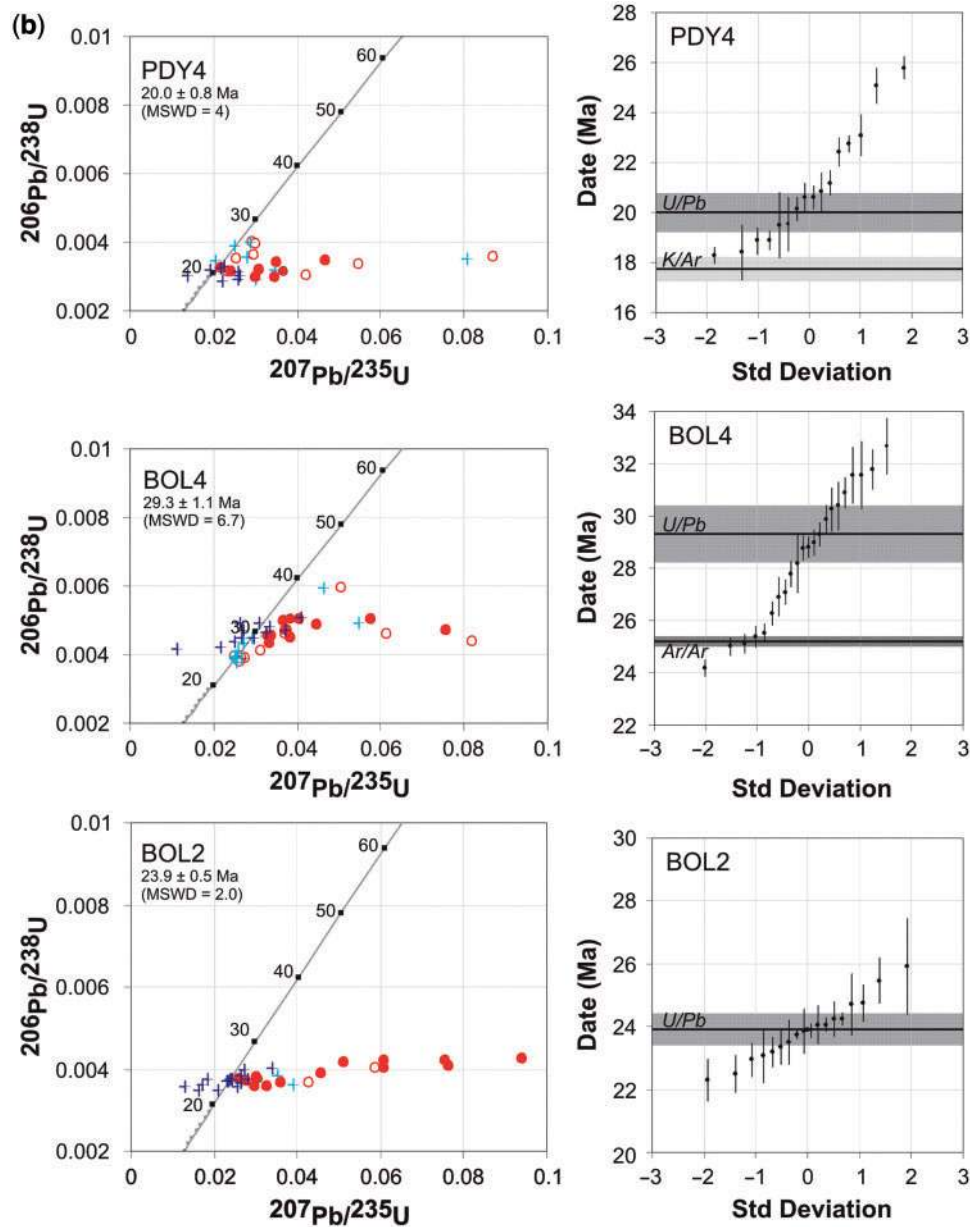
Fig. 3. Continued.

The subjectivity of this process is minimized in the following way. If the entire zircon population for a given sample returns MSWD values substantially greater than unity, then normal probability plots are used to identify outliers and separate populations. Removal of points from a population is terminated when the MSWD of that population drops to that of the monitor standard, usually an MSWD of ~1·5. In this way, grains only 'subtly older' (a couple of million years) can be identified (see Bryan *et al.*, 2004; Allen & Barnes, 2006). Histograms and cumulative probability density function analysis are also particularly

useful in identifying modes in the age distribution (e.g. Charlier *et al.*, 2004; Bacon & Lowenstern, 2005) by taking into account analytical uncertainties on single analyses.

RESULTS

Cathodoluminescence (CL) images (Fig. 5) illustrate that the SMO zircons show many of the complexities and internal structures reported from other large-volume, silicic eruptive units and magmatic systems (e.g. Brown &
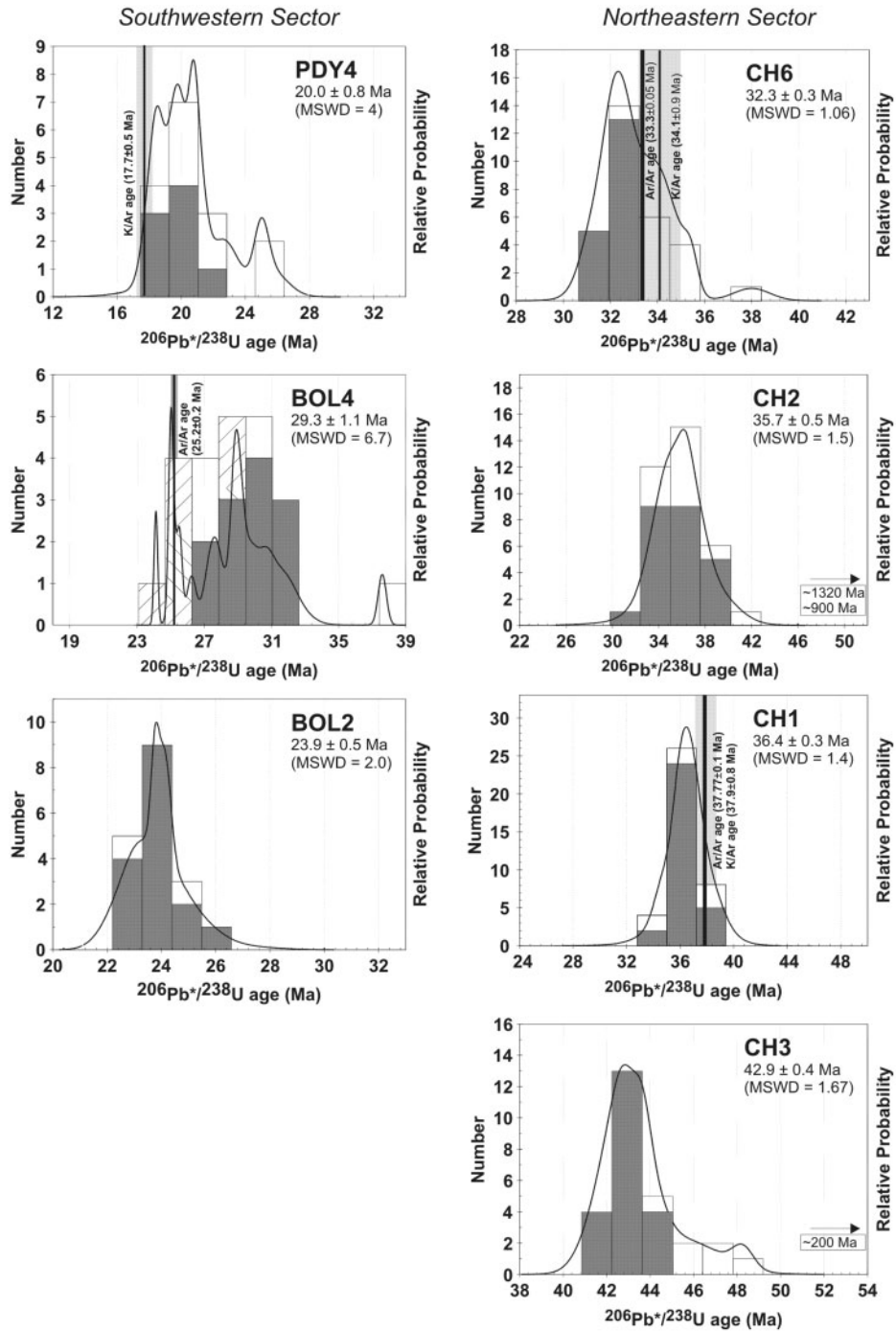
Fig. 4. Cumulative probability density function curves and histograms generated using the probability function in Isoplot (Ludwig, 2002), with samples arranged in relative stratigraphic order for southwestern and northeastern sectors. Dark grey shaded bars denote those U–Pb age analyses used in weighted mean age calculation, unfilled bars are analyses not meeting analytical criteria and omitted from U–Pb age calculation, and the diagonally shaded bars for BOL4 are the distinct suite of U- and HREE-rich zircons (see Figs 5d and 6). Those analyses plotting off the diagram are indicated by an arrow. The oldest ignimbrites from the NE sector have distinctly unimodal probability peaks with positive skewness to some samples, whereas the youngest ignimbrites from the SW sector have more polymodal and complex age distributions in the U–Pb age spectra as exemplified by samples BOL4 and PDY4. K/Ar and unpublished ^{40}Ar/^{39}Ar ages are shown for comparison, with errors given by the shaded envelopes.
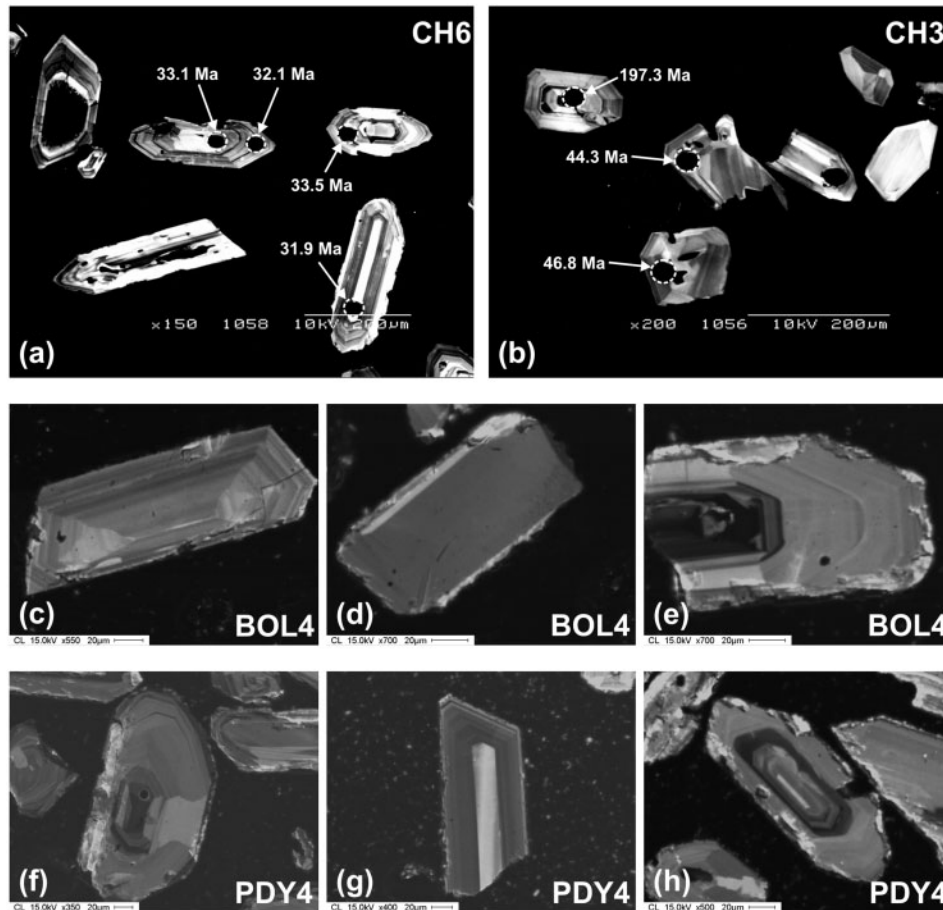
Fig. 5. Cathodoluminescence images of zircons from selected units illustrating the variety in zonation patterns and CL response. (a, b) Sample CH6 (Vista Tuff) and sample CH3, respectively; grains are annotated with locations of laser ablation analysis pits and the corresponding age determination for that location. Dashed circles mark laser ablation pit size. The Early Jurassic age xenocryst core to one zircon grain in (b) should be noted. (c–e) Close-ups of zircon grains from sample BOL4 (Alacrán ignimbrite) with an example of the unzoned and high-U zircons shown in (d) from which U–Pb ages of ∼25 Ma were obtained. (f–h) Selected zircon grains from sample PDY4 illustrating the presence of both light and dark CL core domains (i.e. low and high U, respectively).

Fletcher, 1999; Brown & Smith, 2004; Charlier *et al.*, 2004; Miller & Wooden, 2004). The CL images reveal that most zircons are characterized by fine-scale oscillatory magmatic growth zones, reflecting variations in trace element [U, Th, Y, heavy REE (HREE)] concentrations. Sector zoning is also observed in some grains. Despite their generally euhedral nature, some imaged zircons possess anhedral cores or internal surfaces that truncate and embay into growth zones. Zircons with U-rich (dark CL) and U-poor (bright CL) cores are present in all samples examined (Fig. 5). A glass coating is variably preserved on many grains following the crushing and separation process, indicating that the zircons were in contact with the rhyolite melt prior to eruption.

Northeastern sector

Four samples have been analysed from the Chihuahua region, where several caldera eruptive centres have been identified for the SMO ignimbrites (e.g. Wark, 1991; Wark *et al.*, 1990; Swanson *et al.*, 2006) and Grenville-aged basement is exposed (Ruiz *et al.*, 1988b; James & Henry, 1993; McDowell *et al.*, 1999). Sample CH3 is from the Bellavista Canyon sequence described by McDowell & Mauger (1994), where undeformed and flat-lying rhyolitic ignimbrites overlie a tilted Late Cretaceous volcanic sequence. Two densely welded ignimbrites from this section have been dated by K/Ar at 46·3–44·8 Ma (McDowell & Mauger, 1994). Regionally, ignimbrites dated between 46 and 39 Ma were considered by McDowell *et al.* (1990) to be the first signals of the mid-Tertiary 'ignimbrite flare-up' in Mexico. The CH3 ignimbrite crops out below a succession of undated basaltic andesites that are in turn capped by 29·6–30·6 Ma ignimbrites (McDowell & Mauger, 1994). This plagioclase- and quartz-phyric welded ignimbrite is the oldest unit dated in this study; 22 of 28 analyses meeting analytical criteria give an age of

42·86 ± 0·39 Ma (MSWD = 1·67). Because the location of the sample dated by McDowell & Mauger (1994) is not known, we cannot compare directly our U–Pb age with their K–Ar age. However, CH3 comes from the lower half of the Bellavista Canyon section and the U–Pb age is in accord with the first regional episode of ignimbrite volcanism in the area, and may correspond to a regional pulse of silicic ignimbrite volcanism across the northern SMO at 44·1–45·4 Ma (McDowell & McIntosh, 2007). An inherited component is also present in this sample, with an ∼200 Ma core the most obvious (Fig. 5b). However, five grains dated between 45 and 49 Ma are interpreted as indicating subtle inheritance (see Fig. 4). These grains overlap in age with widespread andesitic to rhyolitic igneous rocks (Lower Volcanic Complex of McDowell & Clabaugh, 1979) with reported ages between 40 and 53 Ma that underlie the main SMO ignimbrite pile (Aguirre-Díaz & McDowell, 1991).

Sample CH1 is from the upper unit of the Gallego Rhyolite, from which a K/Ar age on feldspar of 37·9 ± 0·8 Ma has previously been reported (Keller *et al.*, 1982). The K/Ar age is consistent with two $^{40}Ar/^{39}Ar$ ages of 37·96 ± 0·10 Ma and 37·77 ± 0·10 Ma (laser fusion analyses of multi-crystal aliquots from the same sanidine separates) obtained recently from an ignimbrite sampled to the west and correlated with the Gallego Rhyolite (F. W. McDowell & W. McIntosh, unpublished data). The lava-like Gallego Rhyolite (70·7 wt % SiO_2 on anhydrous basis; Table 4) is crystal-rich, containing up to 50% phenocrysts of oligoclase, sanidine and augite (Keller *et al.*, 1982). Twenty-eight zircon analyses, of which 22 meet analytical criteria, give a $^{206}Pb/^{238}U$ age of 36·4 ± 0·3 Ma (MSWD = 1·4), with single analyses ranging between 34 and 39 Ma (see the Electronic Appendix). The zircons have relatively low U (172 ppm average) and Th (113 ppm average) contents compared with most of the other samples in this study. The U–Pb age is slightly younger than the K/Ar and $^{40}Ar/^{39}Ar$ ages (Figs 3 and 4).

Ignimbrite CH2 is the northernmost ignimbrite in this study and was sampled from a 500 m thick succession ∼20 km north of Sierra el Nido–Sierra Tinaja Lisa where McDowell & Mauger (1994) reported a succession of ignimbrites with a basal ignimbrite dated 36·3 Ma and where Mesozoic marine rocks are exposed. The succession from which CH2 was sampled is also 20–25 km to the west of the San Buenaventura section studied by Albrecht & Goldstein (2000). The CH2 ignimbrite is distinctly porphyritic with abundant quartz and sanidine phenocrysts. Analysed zircons from sample CH2 have low U and Th contents similar to CH1 (see Electronic Appendix). Twenty-three of 36 analyses meeting analytical criteria yield an age of 35·7 ± 0·5 Ma (MSWD = 1·5). Two zircon cores are clearly inherited, one analysis of

Table 4: Major and trace element data for ignimbrites examined in this study

Sample:	NV11	NV01	NV07	SGD2	BOL2	BOL4
Eruptive rock:	Vista	Vista	Vista	Gallegos		Alacran
Unit:	Tuff	Tuff	Tuff	Rhyolite		Ignimbrite
SiO_2	72·37	74·03	75·66	70·71	77·61	70·33
TiO_2	0·29	0·33	0·14	0·53	0·20	0·05
Al_2O_3	15·01	13·96	13·52	14·68	10·79	16·88
Fe_2O_3	2·19	1·92	0·56	1·41	—	—
FeO	0·14	0·12	0·16	1·44	—	—
FeO^T	2·57	1·85	0·67	2·70	2·22	0·84
MnO	0·04	0·07	0·05	0·05	0·05	0·02
MgO	0·55	0·33	0·24	0·38	0·26	0·26
CaO	1·89	1·10	1·41	1·27	0·31	0·20
Na_2O	3·48	4·01	3·62	3·74	2·47	3·58
K_2O	3·98	4·06	4·62	5·69	6·05	7·81
P_2O_5	0·05	0·06	0·01	0·10	0·03	0·03
H_2O^+	1·15	0·94	2·23	2·58	—	—
H_2O^-	0·43	0·07	0·27	0·26	—	—
CO_2	b.d.l.	b.d.l.	b.d.l.	0·01	—	—
LOI	—	—	—	—	0·81	—
Total	99·34	100·48	100·12	96·65	98·93	98·29
Ba	950	1468	388	—	187	45
Rb	149	141	234	279	169	436
Sr	217	153	117	90	26	18
Y	19	31	22	66	54	53
Zr	112	245	83	633	99	92
Nb	10	12	7	52	19	22
Th	18	17	31	—	2	3
Pb	—	—	—	—	10	13
Ga	—	—	—	—	18	33
Zn	41	8	34	—	60	68
Cu	—	—	—	—	1	1
Ni	—	—	—	—	1	1
V	38	13	11	—	6	4
Cr	—	—	—	—	2	3
Hf	4	8	4	—	3	5
Cs	3	6	10	—	2	150
Sc	5	6	3	—	3	1
Ta	1	1	1	—	—	—
Co	4	1	1	—	1	1
U	4	4	10	—	1	3
La	43	46	35	—	37	3
Ce	58	85	55	—	57	9
Pr	—	—	—	—	10	1
Nd	—	—	—	—	37	4
Sm	4	8	3	—	8	2
Eu	1	2	0·4	—	1	0·1

(continued)

Table 4: Continued

Sample:	NV11	NV01	NV07	SGD2	BOL2	BOL4
Eruptive rock:	Vista	Vista	Vista	Gallegos		Alacran
Unit:	Tuff	Tuff	Tuff	Rhyolite		Ignimbrite
Gd	—	—	—	—	9	4
Tb	1	1	0.4	—	1	1
Dy	—	—	—	—	10	8
Ho	—	—	—	—	2	2
Er	—	—	—	—	5	5
Yb	2	3	3	—	5	5
Lu	0.4	1	0.4	—	1	1
M	1.06	1.34	1.41	3.5	1	1
T_{Zr}	780	829	731	749	745	744

Data for the Vista Tuff from Wark (1991) and Gallego Rhyolite from Keller (1977) and Keller *et al.* (1982). Major elements have been normalized to 100 wt % volatile-free with trace elements for the Vista Tuff and Gallego Rhyolite also normalized on a LOI-free basis. The *M* value is the calculated cation ratio of the melt $[(Na+K+2Ca)/(Al \times Si)$; Watson & Harrison, 1983] and T_{Zr} is the zircon saturation temperature (Watson & Harrison, 1983). Major elements for the Bolaños Graben ignimbrite samples have been determined by XRF and trace elements by ICP-MS at the Department of Geochemistry, National Autonomous University of Mexico (see Appendix for analytical details). b.d.l., below detection limit.

which is concordant at ~1320 Ma, the other discordant at ~910 Ma. The older grain age is similar to that obtained from an intermediate orthogneiss xenolith at La Olivina (1370 ± 18 Ma, Rudnick & Cameron, 1991), a U–Pb crystallization age of 1328 ± 5 Ma for a metadiorite exposed near Chihuahua (Blount *et al.*, 1988), and Nd model ages (T_{DM} of 1.77–1.37 Ga) for exposed mafic to intermediate orthogneiss rocks in west Texas and northern Mexico (Ruiz *et al.*, 1988*b*). Two subtly older grain ages of ~40 Ma represent outliers in the age population and were excluded from the U–Pb age calculation for the sample.

Sample CH6 is from the Vista Tuff (Swanson & McDowell, 1985; Wark *et al.*, 1990; Swanson *et al.*, 2006), which is thought to be a caldera collapse-related ignimbrite that produced the ~20 km diameter Las Varas caldera at ~34.1 Ma. Collapse of the Tomochíc caldera was partly superimposed on the Las Varas caldera, with Tomochíc collapse-related ignimbrite eruptions occurring between 32 and 31 Ma (Wark *et al.*, 1990). The reported age for the Vista Tuff of 34.1 ± 0.9 Ma is a mean age of seven K/Ar dates of biotite, plagioclase and alkali feldspar separates that range from 33.1 ± 0.7 Ma to 35.8 ± 0.8 Ma (Wark *et al.*, 1990). More robust eruptive age constraints come from two $^{40}Ar/^{39}Ar$ ages of 33.33 ± 0.05 Ma and 33.41 ± 0.04 Ma (F. W. McDowell & W. McIntosh,

unpublished data), based on multiple fusions of single grains of sanidine.

The Vista Tuff is a moderately to densely welded, crystal-rich (up to 50% phenocrysts) ignimbrite that is petrographically and chemically zoned (72.3–75.6 wt % SiO_2 on an anhydrous basis, Table 4; Wark, 1991). The ignimbrite contains the assemblage plagioclase, quartz, biotite, hornblende, sanidine and Ti-magnetite with trace titanite, zircon, apatite and chevkinite; sanidine and quartz attain higher relative proportions in the stratigraphically lowest samples (Wark, 1991; Swanson *et al.*, 2006). Eighteen of 30 zircon analyses meeting analytical criteria give an age of 32.27 ± 0.29 Ma (MSWD = 1.06). As with the Gallego Rhyolite, the U–Pb age is slightly younger by ~2 Myr than the mean K/Ar age, and ~1 Myr less than the $^{40}Ar/^{39}Ar$ ages (Fig. 3). Some subtle inheritance is indicated in the U–Pb age spectra, with the presence of several grains with ages of ≥34 Ma, and a clear case of inheritance is confirmed by one core–rim pair of analyses with a core age of ~38 Ma and a rim age of ~33 Ma. This core–rim pair indicates that the ~38 Ma zircon core grew before it was introduced into the host magma body when a new episode of zircon crystallization occurred just prior to eruption.

Southwestern sector

In the southwestern sector of the SMO, Early Miocene ignimbrites are dominant, but are probably underlain by an Oligocene ignimbrite sequence, especially in the eastern part of the region, based on the exposure in the southern part of the Bolaños Graben of a package of ignimbrites from which a K–Ar age of 30.1 Ma has been obtained (Ferrari *et al.*, 2002). Two ignimbrite samples were collected from a section within the central part of Bolaños Graben with a vertical separation of ~600 m. The stratigraphically lowest exposed ignimbrite (BOL2) is a red welded, relatively clast-poor, high-silica rhyolite (Table 4) ignimbrite sampled from the Rio Carboneras. The BOL2 ignimbrite lies along strike to the south of a series of reddened welded ignimbrites at the base of the exposed section in the Bolaños district described by Lyons (1988), including the Bolaños Tuff, with a minimum K/Ar age of 22.2 Ma. The ignimbrite contains ~15% phenocrysts, with the assemblage dominated by 1–2 mm long sodic sanidine and quartz. Both the BOL2 and BOL4 ignimbrites are distinctive in having low zircon yields (<1000 grains per 3–4 kg of sample) and small zircon grain sizes (mostly 30–100 μm long) compared with the other studied samples. For BOL2, 16 of 18 analyses meeting analytical criteria yielded an average age of 23.9 ± 0.5 Ma but with a relatively high MSWD of 2.0. The corresponding probability density function curve has a strong asymmetric peak at ~24 Ma but is skewed to higher ages and has a subsidiary population at ~23 Ma (Fig. 4). Compositionally, the dated zircon population is bimodal in terms of U content

with low-U (100–360 ppm) and high-U (∼1000 ppm to 1·3 wt %) groupings (see the Electronic Appendix). Based on the high MSWD, the extreme chemical variation of the zircons, and asymmetric probability density function curve, we interpret the U–Pb age to comprise more than one discrete age population which cannot be clearly discriminated. The U–Pb age is therefore best considered as a maximum age for the emplacement of the BOL2 ignimbrite.

The BOL4 ignimbrite (Alacrán Tuff of Lyons, 1988) is a crystal-poor (∼5 modal %), weakly to non-welded rhyolite ignimbrite that is distinctive for being an example of a fissure-fed ignimbrite (Aguirre-Díaz & Labarthe-Hernandez, 2003). It contains a fine-grained assemblage of quartz, sanidine, oligoclase, biotite, and Fe–Ti oxides (Table 4), and Scheubel *et al.* (1988) noted that some of the sanidine phenocrysts are partially embayed. The U–Pb zircon age of the uppermost ignimbrite dated from the Bolaños section is complicated by the presence of a xenotime-rich population (as a solid solution component in the zircons) recognized in CL imaging (Fig. 5d). U–Pb dating revealed that some of these grains contain up to 1·1 wt % U (see the Electronic Appendix). For sample BOL4, 17 of 22 grains meeting analytical criteria yielded an age of 27·5 ± 1·3 Ma with an unacceptably high MSWD of 24, as indicated by the polymodal probability peaks (Fig. 4), which clearly does not represent one age population. Removal of the xenotime-rich grains, five of which have relatively young ages of ∼25 Ma (Fig. 4), increases the age of the population to 29·3 ± 1·1 Ma; however, the MSWD of 6·7 is still too high to represent a single population. Superficially, the zircon population age is consistent with the known duration of SMO volcanism and the age of the Oligocene pulse of ignimbrite volcanism in the southern SMO from ∼32 to 28 Ma (Ferrari *et al.*, 2002). However, the population age for BOL4 is inconsistent with stratigraphic constraints, given the ∼24 Ma U–Pb zircon age for BOL2 at the base of the section, and previously published K/Ar dates (all <24 Ma) from this section (Lyons, 1988; Scheubel *et al.*, 1988). Of note is that the youngest U–Pb zircon ages obtained from the xenotime-rich zircons overlap an $^{40}Ar/^{39}Ar$ age of 25·2 ± 0·2 Ma (plateau age based on step-heating analysis of a bulk sanidine separate) obtained independently for the Alacrán ignimbrite from the same sample location (M. López & G. Aguirre-Díaz, unpublished data). Importantly, the stratigraphic constraints indicate that the $^{40}Ar/^{39}Ar$ age provides only a maximum age for ignimbrite emplacement, and that the sanidine crystal population may also contain an inherited component.

From a welded rhyolitic ignimbrite sampled from the upper sections exposed in the Rio Santiago (sample PDY4; Table 2), 12 of 16 grains meeting analytical criteria give a mean age of 20·8 ± 1·4 Ma, but with a very

Table 5: K/Ar age data for Group 2 ignimbrite PDY4 from the southern SMO

Sample	Mineral	% K	$^{40}Ar_{rad}$ (nl/g)	% $^{40}Ar_{air}$	Age (Ma) ± 1σ
PDY4	Biotite	4·51	3·058	26·6	17·7 ± 0·5

See Appendix for analytical details.

high MSWD of 134 and several probability peaks in the age data (Fig. 4). A relatively clear case of inheritance exists in the age spectra, with four grain ages between 22·4 and 25·8 Ma. Excluding these four grains, the remaining grains define a single age population of 20·0 ± 0·8 Ma (MSWD = 4·0), but further subdivision is not possible. Biotite from ignimbrite PDY4 was dated by K/Ar (Table 5) to resolve some of the complexities in the U–Pb age spectra and confirm if the U–Pb zircon age provides a useful constraint on the eruption age. The biotite K/Ar age of 17·7 ± 0·5 Ma is one of the youngest ages so far obtained for southern SMO ignimbrite volcanism, and indicates that the zircon U–Pb age, as with BOL4, does not record the age of crystallization from the host magma. Importantly, the comparison of the U–Pb ages with eruptive age constraints provided by the mineral K/Ar and $^{40}Ar/^{39}Ar$ ages for the PDY4 and BOL4 ignimbrites raises the possibility that many southern SMO ignimbrites may be dominated by zircon inheritance signatures such that U–Pb zircon ages do not provide robust constraints on ignimbrite eruptive ages.

DISCUSSION

The U–Pb zircon age data presented above confirms the general age range of SMO magmatism as determined by K/Ar and $^{40}Ar/^{39}Ar$ methods in many previous studies. Where independent eruptive age constraints are available from K/Ar or $^{40}Ar/^{39}Ar$ ages, however, discrepancies exist with the U–Pb age dates (Table 6; Figs 3 and 4). The discrepancies between these different dating techniques are too large to be due to analytical uncertainties, but more probably result from differences in the apparent age of the mineral phases present in the magma (see Bachmann *et al.*, 2007). For the Group 1 ignimbrites dated from the northern SMO, the U–Pb ages (with 2σ errors) are younger by ∼2 Myr and ∼1 Myr in comparison with K/Ar and higher precision $^{40}Ar/^{39}Ar$ ages, respectively, and the U–Pb age spectra are dominated by well-defined unimodal probability density function peaks (Fig. 4). We interpret this discrepancy to indicate that some excess Ar is contributing to the bulk feldspar age spectra possibly via the presence of xenocrysts, which is not resolvable by K/Ar or $^{40}Ar/^{39}Ar$ bulk dating methods. In contrast, for the Group 2 ignimbrites from the southern SMO,

Table 6: Summary of age data for seven rhyolite ignimbrite samples analysed in this study

Sample	K/Ar, ^{40}Ar/^{39}Ar age* (Ma) $\pm 1\sigma$	U–Pb age (Ma) $\pm 2\sigma$	N	n	MSWD	Inherited zircon ages (Ma)
Group 1, Northeastern sector						
CH1	37·9 ± 0·8 (san)	36·4 ± 0·3	28	22	1·44	*39*
	37·96 ± 0·1* (san)					
	37·77 ± 0·1* (san)					
CH2		35·7 ± 0·5	36	23	1·5	*40*, 900, ~1320
CH3		42·86 ± 0·39	28	22	1·67	*45–48*, ~200
CH6	34·1 ± 0·9	32·27 ± 0·29	30	18	1·06	*34–35, 38*
	(san, pl ± bio)					
	33·33 ± 0·05* (san)					
	33·41 ± 0·04* (san)					
Group 2, Southwestern sector						
PDY4	17·7 ± 0·5 (bio)	20·0 ± 0·8	16	8	4	*~20–26*
BOL4	25·2 ± 0·2* (san)	29·3 ± 1·1	22	12	6·7	*~26–37*
BOL2		23·9 ± 0·5	18	16	2	*~24–26*

K/Ar ages from Keller *et al*. (1982) and Wark *et al*. (1990); ^{40}Ar/^{39}Ar ages (denoted by asterisk) are unpublished data of G. Aguirre-Díaz & M. Lopez (Alacrán ignimbrite, BOL4) and F. W. McDowell & W. McIntosh (Gallego Rhyolite, CH1; Vista Tuff, CH6). The K/Ar age for the Vista Tuff (CH6) is a mean of seven K/Ar ages obtained from biotite, plagioclase and alkali feldspar separates (Wark *et al*., 1990). *N*, total number of analyses; *n*, number of analyses meeting analytical criteria from which population age is determined. Italicized inherited zircon ages denote antecryst ages. san, sanidine; pl, plagioclase; bio, biotite.
*

the U–Pb ages are distinctly older by 2–4 Myr in comparison with available eruptive age constraints, and have more complex, polymodal U–Pb age spectra (Fig. 4). In these cases, we consider that the U–Pb age spectra are largely dominated by inherited ages. Although the inherited ages provide few meaningful constraints on the age of zircon crystallization from the host magma body and the consequent eruption age, they do provide important information on the ages of crustal source materials and contaminants.

In detail, the zircon age data can be subdivided into three age populations: (1) an age population reflecting crystallization within the magma body immediately prior to eruption (phenocrysts); (2) crystals with substantially older ages ranging from ~200 Ma to 1320 Ma, which are clearly xenocrystic in origin; and (3) an age population more difficult to discriminate from phenocrysts that ranges in age up to 10 Myr older than the interpreted eruption age. The last age population can further be subdivided into those that overlap in age with the duration of eruptive activity of the SMO (38–20 Ma), and those that overlap in age with precursor andesitic to rhyolitic magmatism of Eocene age (Aguirre-Díaz & McDowell, 1991; Ferrari *et al.*, 2007).

Zircon phenocrysts, antecrysts and xenocrysts

Several recent petrological studies have highlighted the potentially significant contribution of earlier formed crystals that are remobilized and incorporated into erupted magma batches, the distinction of which becomes important when attempting to constrain magma residence times and the formation and dynamics of large silicic magma reservoirs (e.g. Bindeman *et al.*, 2001; Gardner *et al.*, 2002; Vazquez & Reid, 2002; Bachmann & Bergantz, 2003; Charlier *et al.*, 2004; Miller & Wooden, 2004; Bacon & Lowenstern, 2005). Crystals in volcanic rocks have traditionally been distinguished into two populations: (1) phenocrysts, which have crystallized from the surrounding melt (glass) in which they were erupted; (2) xenocrysts, which have not crystallized from the host magma and are therefore foreign to the host magma.

Phenocrysts and xenocrysts can have marked textural, chemical and, in particular, age differences, allowing these crystal populations to be readily distinguished. The presence of commonly thick magmatic overgrowths to cores that may be xenocrystic indicates that the core material is more likely to be unmelted zircon from the source region than accidental xenocrysts eroded from the conduit during or immediately prior to the eruption. The Mesozoic and Proterozoic zircon grain ages obtained from samples CH2 and CH3 are obvious examples of xenocrysts in the dataset (see the Electronic Appendix). A new term 'antecryst' was recently used by Charlier *et al.* (2004), following Hildreth (2001), to describe crystals that predate the assembly, crystallization and eruption of the

host magma, but have an origin related to older phases of similar magmatism. The age distinction of antecrysts from phenocrysts is therefore dependent on: (1) the onset and duration of magmatism in the area, which for a volcano could be up to 10^6 years and at a provincial scale $>10^7$ years; and (2) the frequency of magma production, storage and emplacement (either as intrusions or eruptions) causing crystallization events. At 'hyperactive' volcanoes such as Taupo, where magma production and eruption rates are very high, the age difference between antecrysts and phenocrysts may be very small (≥ 40 kyr; Charlier *et al.*, 2004). However, for a region of more protracted magmatism, such as the SMO, antecryst ages can potentially predate phenocryst age populations by up to 10 Myr or more. Consequently, in regions of long-lived magmatism such as western Mexico, or in the absence of high-precision geochronological data, distinguishing phenocrysts from antecrysts, and antecrysts from xenocrysts may be extremely difficult.

Several characteristics in the zircon age and chemical data, as well as textural differences such as in zoning patterns, grain morphology and CL response, can be used to help discriminate phenocryst, antecryst and xenocryst populations. Charlier *et al.* (2004) interpreted bimodal peaks in probability density function curves of zircon age data to indicate remobilization of zircons from an earlier-formed crystal mush (older age peak) and zircon

crystallization from the host magma body in the immediate build-up to eruption (younger age peak). In addition, our data suggest that in more complex cases where magmatism has been protracted in a region over millions to tens of millions of years, broad or polymodal probability peaks (BOL4, PDY4; Fig. 4) are also diagnostic of antecrystic populations being present. Positively skewed and asymmetric age probability curves (e.g. CH3, CH6; Fig. 4) indicate that a subordinate population of antecrystic zircons is present in the sample (see also Bacon & Lowenstern, 2005). Well-defined unimodal peaks in the age data, the age of which is also close to the eruption age, will best represent the crystallization age of zircon phenocrysts from the host magma.

Chemical data obtained during age dating of the zircon grains provide an additional means to assess whether dated zircons may be antecrysts–xenocrysts or phenocrysts (Fig. 6). The Mesozoic and Proterozoic xenocrystic zircons are distinguished chemically by their high Pb contents (>20 ppm) as a result of radiogenic in-growth, but are otherwise compositionally indistinguishable (see the Electronic Appendix). Zircon grains that yield ages consistent with them being phenocrysts are distinctive in all dated samples by having U abundances <1000 ppm and low HREE contents (e.g. Lu <200 ppm). All but one zircon phenocryst from ignimbrites of the northeastern sector have U contents <700 ppm ($n = 95$). Zircons from
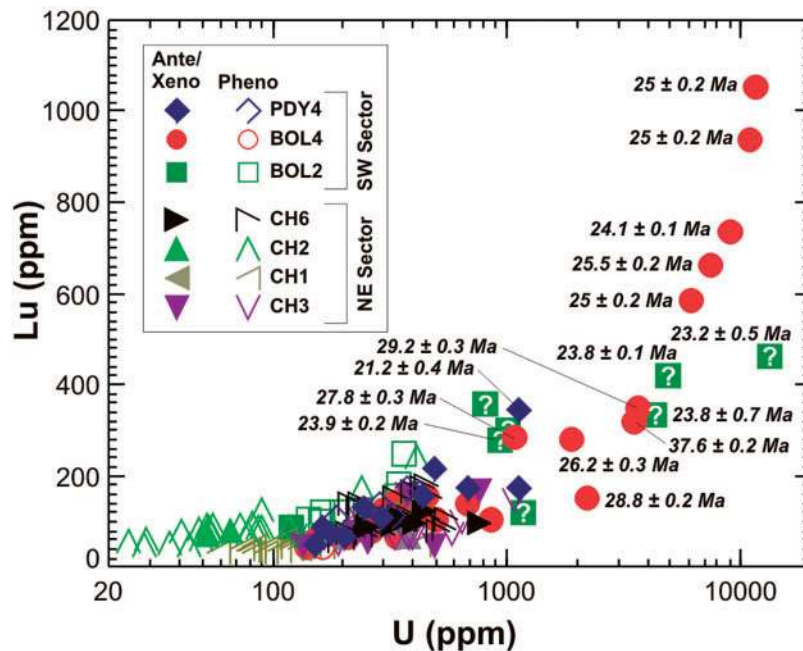
Fig. 6. Zircon trace element chemistry illustrated in a plot of Lu vs U content. Zircon grain compositions are distinguished into phenocrysts (pheno; open symbols) and xenocrysts (xeno) or antecrysts (ante; filled symbols). The positive correlation in Lu (as a proxy for HREE) with U content, which is developed to extreme levels in the high-U zircons of the BOL2 ignimbrite and Alacrán ignimbrite (sample BOL4), should be noted. Single age analyses are annotated for the distinctive high-U antecryst zircons. For BOL2, several high-U zircons are inferred to be antecrysts (queried symbols). Low-U content zircons are developed in the lava-like Gallego Rhyolite (sample CH1) and ignimbrite CH2, whereas the bulk of analysed zircons have U contents between 100 and 1000 ppm. Number of analyses is 180.

the southern SMO ignimbrites, in contrast, show the most chemical variety, evident in their U and HREE abundances (Electronic Appendix), with a distinct population characterized by U $\geq$1000 ppm and Lu $\geq$200 ppm (Fig. 6). Significantly, several high-U zircons in the different ignimbrites of the southern SMO have very similar chemistries, but very different U–Pb crystallization ages. The Bolaños Graben ignimbrites (BOL2, BOL4) show the most extreme zircon chemical variation in U (100 ppm to 1·3 wt %) and Lu (45 to >1000 ppm). The Alacrán ignimbrite (BOL4) has a very distinctive suite of ∼25 Ma high-U, HREE-rich inherited zircons (Fig. 5d), whereas the high-U zircons in the underlying BOL2 ignimbrite cluster in age at ∼23·8 Ma (Fig. 6). We interpret these chemically distinct zircons with U contents >1000 ppm to be antecrystic in origin, but those in BOL2 record different crystallization ages and events from the chemically similar antecrystic zircons in the overlying Alacrán ignimbrite.

At Taupo, zircons with higher U (up to 6000 ppm) and Th (up to 11 000 ppm) contents correspond to peaks in zircon crystallization ages and hence, magma crystallization events (Charlier *et al.*, 2004). In a comparative study of zircons from a variety of igneous suites, Belousova *et al.* (2002) found that the most pronounced HREE enrichment in zircons occurs in pegmatitic rocks, and only zircons from felsic granitoid rocks contain the high U contents observed here. Hydrothermal zircons, precipitated from fluids expelled from the magmas during the final stages of crystallization, are also known to be enriched in trace elements such as U, Th, Y and REE, but are texturally distinct from magmatic zircon (Hoskin, 2005). On the basis of our data, we suggest that at least for the SMO, high U (>1000 ppm) and HREE contents may be a diagnostic feature of antecrystic zircons remobilized from partially to completely solidified crystal mushes of highly differentiated silicic magmas. Importantly, the majority of the analysed zircon antecrysts (39 out of 51), distinguished on the basis of their U–Pb age and statistical analysis show no observable chemical or textural distinction from phenocrysts. Independent chronostratigraphic constraints, high-precision analyses and large datasets to distinguish antecrystic and phenocrystic populations through statistical and cumulative probability density function analysis are therefore important in the interpretation of U–Pb ages of rhyolitic volcanic rocks.

Xenocryst–antecryst entrainment in SMO rhyolites

Xenocrystic (and antecrystic) zircon are not present in all of the rhyolites. Assuming that undersampling can be confidently rejected, the controlling factors on the presence or absence of inherited zircon include: the temperatures of crustal fusion, the composition, degree of zircon saturation and residence time in the host magma, disaggregation of the host rock through significant degrees (tens of volume per cent) of melting, zircon size and source rock composition (Watson & Harrison, 1983; Watson, 1996; Miller *et al.*, 2003; Charlier *et al.*, 2004; Bacon & Lowenstern, 2005). Source rock composition may be particularly important where the magma source lacks zircon (as a result of previous melt depletion events or its mafic composition), or where the ages of crustal sources and magmas are indistinguishable.

To understand the textural characteristics of zircons (e.g. resorption or embayment features) and why some closely related silicic eruptions may have drastically different zircon abundances, several studies have investigated the degree of Zr saturation for erupted magmas by comparing the zircon saturation temperatures based on the model of Watson & Harrison (1983) and magmatic temperatures determined from phenocryst compositions. It has been shown that zircon abundances and their consequent ages show a correlation with the degree of Zr saturation of the magma (Chappell *et al.*, 2000; Miller *et al.*, 2003; Charlier *et al.*, 2004; Bacon & Lowenstern, 2005). Zr-undersaturated magmas [where the magmatic temperature exceeds T_{Zr}, the zirconium saturation temperature of Watson & Harrison (1983)] will not have crystallized zircon, and if zircons are present, they will be xenocrystic or antecrystic in origin. Zircon preservation therefore requires either rapid eruption, the magmas to be only marginally Zr-undersaturated and/or have experienced only a brief temperature excursion to Zr undersaturation to limit magma residence time for dissolution, or protection by occurring as inclusions in other phenocryst phases. Zr-oversaturated magmas (where magmatic temperature is below T_{Zr}) have zircon age populations reflecting crystallization from the host magma. The implication is that, in this case, zircon crystallization from the host magma may overwhelm any inherited zircons present, making detection of a xenocrystic or antecrystic component difficult (Charlier *et al.*, 2004).

The Group 1 ignimbrites from the northern SMO have a small component of crust-derived zircons, representing $\leq$20% of the dated grain population (Fig. 7). The lava-like Gallego Rhyolite ignimbrite (CH1) is an exception to this suite of samples in that no xenocrystic zircons were detected, although two grains dated at ∼39 Ma are likely to be antecrysts. It has a very well-defined unimodal age distribution (Fig. 4) of relatively low-U (Fig. 6) and low-Th zircons, which are consistent with crystallization at high temperatures (Rubatto & Hermann, 2007). The lack of inherited zircon is likely to be because the magma had a temperature greatly exceeding T_{Zr}, resulting in Zr undersaturation and extensive dissolution of any inherited zircon, such that much of the age information on the source region has been lost.

The BOL4 (Alacrán ignimbrite) and PDY4 ignimbrites from the southern SMO, in contrast, have much larger proportions of entrained antecrysts (Fig. 7) based on the significant age discordance between the U–Pb zircon and associated $^{40}Ar/^{39}Ar$ and K/Ar ages, polymodal age distributions and zircon chemistry. A similarly high antecrystic zircon content is suspected for the BOL2 ignimbrite, but at present, we do not have independent constraints on the eruption age, or robust means with which to further discriminate antecrystic from phenocrystic zircons. A significant antecrystic zircon population is indicated to be present in BOL2 based on the similarities in zircon composition to BOL4, the relatively high MSWD on the population age, and the corresponding probability density function curve for BOL2 being

skewed to older ages (Fig. 4). These southern SMO ignimbrites may contain almost entirely inherited antecrystic zircon, as little to no new zircon crystallized from the host magma, which was Zr undersaturated. This is confirmed for the BOL2 and BOL4 ignimbrites where comparison of magma temperature estimates with T_{Zr} (Table 7) reveals that the BOL2 and BOL4 magmas were marginally Zr undersaturated. Consequently, for these ignimbrites, the zircons date primarily the crustal materials involved in partial melting and/or crystal mush remobilization, because there has been little to no new zircon growth in the magma chamber. The inheritance-dominated U–Pb age spectra for these ignimbrites reinforce the importance of field studies and stratigraphic control on sampling and age interpretation.

Age of crust involved in SMO rhyolite petrogenesis

The U–Pb zircon age data give the first direct information on the crustal materials contributing to SMO rhyolite generation. Xenocrystic zircons in the oldest and northernmost rhyolite ignimbrites represent a small component of the age spectra (Figs 4 and 7), but exhibit a considerable range in age from Eocene through Mesozoic to Proterozoic (see the Electronic Appendix). Out of 122 zircon analyses from the four ignimbrites in the northeastern sector, we have found no evidence for the entrainment in the rhyolite magmas of Palaeozoic age zircons derived from sedimentary rocks, and no confirmation of the involvement of paragneissic crust in SMO rhyolite petrogenesis (see Smith et al., 1996). Given the nature of the crustal profile beneath the northern SMO (Fig. 2), the Proterozoic zircons are interpreted to have been derived from gneissic rocks at lower to mid-crustal levels. Of significance is that the ~200 Ma xenocrystic zircon core age from sample CH3 corresponds in age to Jurassic subduction-related magmatism in Mexico (Nazas arc of Bartolini, 1998) and
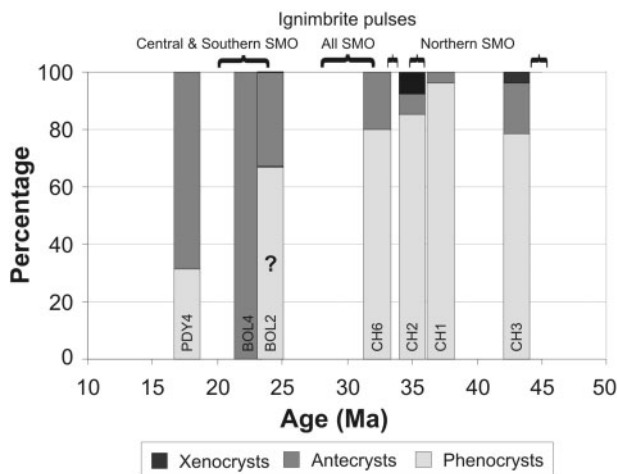
Fig. 7. Histogram illustrating the relative proportions of phenocrysts, antecrysts and xenocrysts in the ignimbrites (see Electronic Appendix) vs eruption age. Peaks in eruptive pulses (32–28 Ma and 24–20 Ma) for the SMO (from Ferrari et al., 2002, 2007) and for the northern SMO (McDowell & McIntosh, 2007) are also shown.

Table 7: Summary of geothermometry estimates for ignimbrites examined in this study

Eruptive unit	Sample no.	Fe–Ti oxides		Feldspars		Biotite	Zr saturation
		$T\,^{\circ}C$	log $f(O_2)$	$T\,^{\circ}C$ (1 kbar)	$T\,^{\circ}C$ (5 kbar)	T (°C)	T (°C)
Vista Tuff	NV01			683, 700	713, 730		829
Vista Tuff	NV07			748	780		731
	BOL2	774	−13·4				745
Alacrán Ignimbrite	BOL4	727	−11·8	760	786	744	744

Data for the Vista Tuff from Wark (1991). Temperature and oxygen fugacity estimates from coexisting Fe-Ti oxides follow the method of Ghiorso & Sack (1991), and oxide mineral pairs used for calculation pass the Mg/Mn partitioning test of Bacon & Hirschmann (1988). Equilibration temperatures from coexisting feldspars in BOL4 were determined with the SOLVCALC 1.0 software of Wen & Nekvasil (1994) using the feldspar site mixing model of Fuhrman & Lindsley (1988), which has stated uncertainties of ±30°C. Temperature estimates obtained from biotite used the geothermometer of Luhr et al. (1984). Zircon saturation temperature estimates based on Watson & Harrison (1983).

implies an eastward extension to the region of known sub-duction-related magmatism at this time (Fig. 1). Mesozoic age xenocrystic zircons (∼200 Ma and 170–180 Ma) have also been reported from mid-Tertiary intermediate orthogneiss xenoliths at the La Olivina locality at the eastern edge of the SMO (Rudnick & Cameron, 1991). In the xenolith, the 200 Ma zircon core had a magmatic rim age of 37 Ma, which is consistent with the findings here of some relatively young, Mesozoic crustal contributions to mid-Tertiary rhyolite magma genesis.

The age and high proportion of inherited antecrystic zircons present in the youngest rhyolite ignimbrites (BOL2, BOL4, PDY4) indicate the involvement of different crustal materials in the generation of the Early Miocene rhyolite magmas of the southern SMO. The antecryst zircon ages in these ignimbrites overlap the age range of magmatism within the SMO (∼38–20 Ma), and are likely to have been sourced from either crystal mushes or solidified plutonic rocks formed during earlier phases of SMO magmatism. In particular, the distinctive high-U and high-HREE characteristics of zircons from the BOL2 and BOL4 ignimbrites are likely to have been recycled from earlier formed, highly differentiated and unexposed plutonic to pegmatitic rocks or crystal mushes probably residing in the upper crust. Although Early Miocene ignimbrites dominate the exposed stratigraphy, an older Oligocene sequence is considered to underlie the region (Ferrari *et al.*, 2002).

The antecrystic zircon ages give some insight into whether they have been remobilized from crystal mushes or solidified plutonic rocks. The relatively close correspondence between inferred eruption ages and the ∼25 Ma and ∼24 Ma high-U antecryst zircon populations in the BOL4 and BOL2 ignimbrites, respectively, suggest these antecrystic zircon populations could have been remobilized from crystal mushes or partially solidified crystal-rich root zones to the magma bodies. However, the spread of antecryst grain ages (∼37·5–24 Ma) and modes (∼25, ∼29 Ma) in the age distribution (Fig. 4) for BOL4 also suggest recycling from a number of temporally distinct and solidified intrusions. Importantly, the antecryst zircon ages are sufficiently old to preclude them from recording prolonged magma residence times (10^4–10^5 years) or even punctuated episodes of zircon growth and rhyolite magma generation from a larger magma system or root zone (e.g. Reid *et al.*, 1997; Brown & Fletcher, 1999; Vazquez & Reid, 2002; Miller & Wooden, 2004; Charlier *et al.*, 2004; Simon & Reid, 2005).

An important implication of our data is that the age (and hence compositional and isotopic) range of crustal materials involved in SMO rhyolite genesis is greater than previously considered (Proterozoic and Palaeozoic orthogneisses and paragneisses, Ruiz *et al.*, 1988*b*; Wark, 1991; Smith *et al.*, 1996). The presence of Eocene and rare Early Jurassic age zircons probably reflects inheritance from igneous basement (Fig. 2) generated during preceding phases of subduction-related activity (Aguirre-Díaz & McDowell, 1991; Jones *et al.*, 1995; Busby-Spera, 1998; Dickinson & Lawton, 2001), such that the fertility of the lithosphere beneath the SMO was probably increased by geological events prior to the ignimbrite flare-up (Ferrari *et al.*, 2007). Humphreys *et al.* (2003) proposed that the coeval, widespread and voluminous mid-Tertiary silicic-dominated magmatism of the Basin and Range Province to the north of the SMO was a response to hydrated lithosphere being exposed to asthenospheric mantle uprise, with hydrated and fertilized lithosphere developing during prior flat-slab subduction of the Farallon plate (Laramide orogeny). We suggest that remelting of young crustal materials and a hydrous igneous underplate or crustal intrusions (e.g. Tamura & Tatsumi, 2002) generated during earlier episodes of subduction may therefore have been the controlling process in producing the calc-alkaline geochemical and relatively unradiogenic isotopic signatures of the SMO rhyolites.

Long-term temporal–compositional variations as evidenced from zircon inheritance patterns

The degree and age of inherited zircon varies markedly, both spatially and temporally, for the ignimbrites examined in this study. The most prominent feature of the U–Pb age data in Fig. 4 is the up-sequence change from well-defined unimodal probability density function peaks to more complex polymodal age distributions in the youngest ignimbrites. This change reflects the increasing inheritance of antecrystic-type zircons in the Early Miocene ignimbrites of the southern SMO (Fig. 7). This trend towards more antecrystic-type zircons suggests the reworking of igneous rock formed during earlier phases of SMO magmatism. The continued injection of basalt is predicted to lead to remelting of previously intruded magma (Annen & Sparks, 2002). It is noteworthy that rhyolites in the Deccan and Karoo flood basalt provinces have been interpreted as remelts of an earlier-formed mafic igneous underplate, based on isotopic similarities to the associated flood basalts (Cleverly *et al.*, 1984; Lightfoot *et al.*, 1987). The large-scale recycling of SMO-age zircons into the youngest rhyolite ignimbrites may be a record of a similar process. Crustal melting during the culminating phases of southern SMO magmatism (∼24–20 Ma; Ferrari *et al.*, 2002) may have occurred in crust that had been largely replaced by broadly coeval igneous intrusions, or occurred at very shallow levels within the volcanic pile (e.g. Bindeman *et al.*, 2001). However, at present, our data cannot fully resolve whether this trend is the result of changing source composition and/or depth of melting.

Implications for SMO rhyolite petrogenesis

Silica-rich magmas can be products of extreme crystal fractionation of basaltic magmas at low pressure, but these are small in volume with respect to the mantle-derived parent. To generate large volumes of silica-rich magmas as in the SMO and typical of the SLIPs in Table 1, however, interpretations have typically been polarized into two end-member models. In the first model, mantle-derived basalt provides heat and some mass contribution to the erupted rhyolite, but the crust is the source of most material (e.g. Huppert & Sparks, 1988; Ruiz et al., 1988a, 1990; Ewart et al., 1992; Pankhurst & Rapela, 1995). Both numerical and experimental models have shown that crystallizing basaltic melts can easily provide sufficient heat energy to melt the surrounding country rock such that relatively large amounts of silicic melt can be generated over geologically short time scales when there is an external heat supply, and that mobilization of large quantities of crustal melt requires repeated intrusion for basaltic underplating to be effective (Huppert & Sparks, 1988; Bergantz, 1989; Barboza & Bergantz, 1998; Patiño Douce, 2000; Annen & Sparks, 2002; Dufek & Bergantz, 2005). Furthermore, continued basalt injection is predicted to lead to remelting of formerly intruded igneous rock (Annen & Sparks, 2002), aided by an elevated geotherm caused by the prolonged history of basaltic flux. In the second model, rhyolite is seen primarily as the end-product of basalt differentiation, although limited crustal input is often required by isotopic constraints (Cameron & Cameron, 1985; Wark, 1991; Smith et al., 1996). Both models appear to satisfactorily explain, to a first order, the whole-rock geochemical and isotopic characteristics of the rhyolites and granites.

Models of crustal assimilation combined with fractional crystallization (AFC) have been used by many workers to explain rhyolite genesis in the SMO (e.g. Cameron & Cameron, 1985; Wark, 1991; Smith et al., 1996); as well as by other workers for the Taupo Volcanic Zone (McCulloch et al., 1994; Graham et al., 1995) and for the 'ignimbrite flare-up' of the western USA (Johnson, 1991; Perry et al., 1993, and references therein). It is envisaged that basaltic magmas ascend into the lower crust, where crustal assimilation leads to the generation of basaltic andesitic to andesitic magma compositions in a MASH zone (Hildreth & Moorbath, 1988). Specifically for the SMO, AFC modelling indicates that rising batches of crustally contaminated andesitic magma could produce rhyolite compositions without further crustal input, via closed-system fractional crystallization in crustal reservoirs, such that the rhyolite magma end-products generally had minimal (<10–20%) crustal contributions (Wark, 1991). Important implications of these types of models are that: (1) the volume of parental basaltic magma required to produce the large volumes of rhyolites is 4–5 times greater than the volume required for crustal partial melting-dominated models where the ratio of intruded or underplated basalt to erupted rhyolite is ∼1:1 (Ruiz et al., 1988a); (2) large masses of crystal cumulate material (>50%) are generally required to have been removed to produce the least evolved rhyolite compositions (Wark, 1991), and, for the SMO, fractional crystallization of mafic magmas is expected to have produced a ∼4 km thick underplate of feldspar-rich cumulate material (Cameron et al., 1980a; Cameron & Hanson, 1982; Ruiz et al., 1988a); and (3) melt depletion of the crust will be limited and the pre-existing crustal materials should have retained their chemical and isotopic characteristics and degree of fertility following magmatism.

The presence and age of the inherited zircon crystals in the SMO rhyolites examined here provide new constraints for interpreting the petrogenesis of the rhyolites. The crustally contaminated basaltic andesite–andesite magmas that are parental to the rhyolites in AFC models (Wark, 1991), and erupted coevally with the SMO rhyolites (Cameron et al., 1989; Wark, 1991), are strongly Zr undersaturated (Fig. 8). Consequently, evolution of these parental magma compositions in a closed system (Wark, 1991) toward rhyolitic compositions is highly unlikely to preserve any entrained zircons in the rhyolitic magmas (Watson, 1996; Charlier et al., 2004). To demonstrate this, we have followed the same approach as Charlier et al. (2004) by estimating zircon dissolution time-scales using the zircon dissolution–growth model of Watson (1996). Rates of zircon dissolution have been estimated for a range of compositions from (inferred parental) basaltic andesite to rhyolite from the Tomochic volcanic centre in the northern SMO, which have previously been interpreted as genetically related via AFC models (Wark, 1991), and for the Bolaños Graben ignimbrites that have high abundances of antecrystic zircon (Fig. 7).

The strong Zr undersaturation of the mafic magmas (Fig. 8) is reflected by the very rapid rates of zircon dissolution, even for the largest zircons ($\leq$1 year, Table 8). Zr saturation is reached only in the rhyolites (>70 wt % SiO_2, Fig. 8), such that entrained zircons in dacitic magmas are also predicted to dissolve rapidly (10^1–10^2 years, Table 8). In detail, the rhyolites show some variation from Zr oversaturation (e.g. NV01, Vista Tuff; Table 7) to marginal Zr undersaturation (e.g. BOL2, BOL4); however, in these cases dissolution rates are greatly reduced (Table 8), such that entrained zircon xenocrysts and/or antecrysts should be preserved in magmas that reside in crustal magma chambers over time scales of 10^3–10^5 years.

Zircon inheritance has been observed during this study in one SMO rhyolite for which the degree of zircon saturation can be assessed (CH6 of Table 2, Vista Tuff of Swanson & McDowell, 1985), and which also forms part
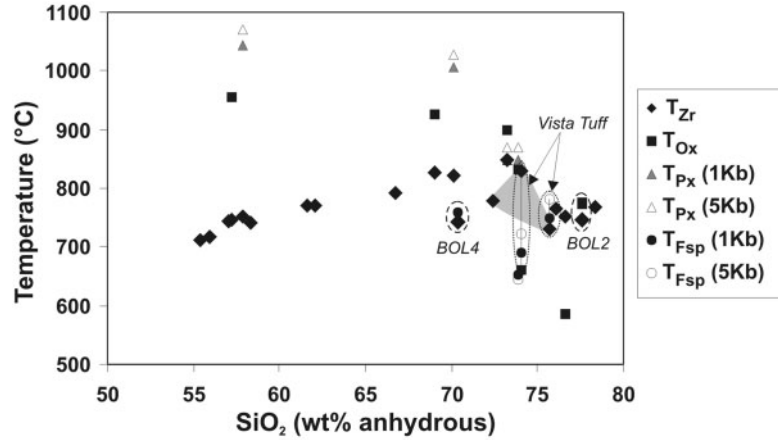
Fig. 8. Plot of temperature estimates vs whole-rock silica composition for a suite of andesitic to high-silica rhyolite volcanic rocks from the Tomochic area, northern SMO (Wark, 1991) and the Bolaños ignimbrites (BOL2, BOL4) from the southern SMO. Zircon saturation temperatures (T_{Zr}; Watson & Harrison, 1983) have been calculated in this study for the Tomochic suite from whole-rock chemical data of Wark (1991). Corresponding magmatic temperature estimates from Fe–Ti oxides (T_{Ox}), two pyroxenes (T_{Px}) and two feldspars (T_{Fsp}) are also from Wark (1991; see also Table 7), with the pyroxene and feldspar temperatures calculated at different pressures (●, 1 kbar; ○, 5 kbar). The shaded field denotes the range of zircon saturation temperatures for the compositionally zoned Vista Tuff (Table 4; our sample CH6), and tie-lines join temperature estimates for two Vista Tuff samples (NV01, NV07 of Wark, 1991) enclosed by dotted lines. The corresponding zircon saturation and magmatic temperature estimates for BOL2 and BOL4 are enclosed by dashed lines.

Table 8: Results of zircon dissolution modelling following the approach outlined by Charlier et al. *(2004)*

Sample	Lithology	SiO₂ (wt %)	Zr (ppm)	Magmatic T (°C)	T_{Zr} (°C)	Initial radius (μm)	Time to disappearance (years)
O54	Magdalena basaltic andesite	57·85	185	1045	753	100	0·03
						250	0·22
N70	Lagunitas basaltic andesite	57·24	165	980	745	100	0·17
						250	1·03
O38	Magdalena dacite	69·05	267	925	828	100	32·6
						250	203
NV07	Vista Tuff	75·66	83	750	731	100	9191
						250	57041
BOL2	High-silica rhyolite ignimbrite	77·51	99	774	745	100	2612
						250	16292
BOL4	Alacrán ignimbrite	70·29	92	760	744	100	7533
						250	46407

Geochemical data and magmatic temperature estimates for samples O54, N70, O38 and NV07 from Wark (1991). Values for melt viscosity were based on Vetere *et al.* (2006) for the andesites, and Hess & Dingwell (1996) for the silicic rocks. Estimated water contents were 2 wt % for the basaltic andesites, 3 wt % for the dacite, and 4 wt % for the rhyolites. Dissolution rates in the various melt compositions are for spherical zircon crystals.

of the igneous suite modelled by Wark (1991) as being related by AFC. Several antecrystic zircons are present (Figs 4 and 7) with grain ages >34 Ma (Table 6). One zircon has an antecrystic core age of ~38 Ma and a magmatic rim age of ~33 Ma, indicating that antecrystic zircon was incorporated into the magma with negligible dissolution, and subsequently had new growth. The degree of Zr saturation in the compositionally zoned Vista Tuff varies from slightly negative to positive (Fig. 8); however, dissolution rates are much reduced, resulting in long predicted residence times for any entrained zircon xenocrysts and antecrysts (Table 8). The southern SMO ignimbrites, in contrast, appear to have remained sufficiently Zr undersaturated to limit new zircon crystallization; the degree of Zr undersaturation was neutral to slightly negative, resulting in sluggish dissolution rates

(Table 8) and the preservation of a high proportion of sub-hedral to euhedral antecrystic zircons (Fig. 5).

For the SMO rhyolites examined in this study, and particularly those that contain inherited zircons, we conclude that the magmas either had to be erupted rapidly enough, or had to be sufficiently evolved (i.e. high Zr concentrations) so that the entrained zircons could survive. Rapid eruption is inconsistent with a model of closed-system and prolonged fractionation requiring >50% mass removal of crystals to produce the rhyolites (Cameron *et al.*, 1980*a*; Wark, 1991). Our data cannot exclude lower crustal contamination of mafic magmas, which have no zircon record of crustal interaction as a result of the strong Zr undersaturation of the magmas, but at the very least require further crustal assimilation in silicic magmas where the degree of Zr undersaturation is at most only weakly negative. The presence of a significant component of crust-derived zircon xenocrysts and ante-crysts indicates that the rhyolites examined in this study, and we suspect for the majority of SMO rhyolites, cannot have evolved by prolonged closed-system fractionation following early lower crustal assimilation (and therefore zircon entrainment) to produce basaltic andesite–andesite parental magma compositions. We support the conclusions of Charlier *et al*. (2004) that the presence of entrained zircons in rhyolites requires large-scale melting and disaggregation of crustal protoliths. A greater role for crustal melting of young igneous crustal materials is implied by our zircon age data, with superimposed fractional crystallization.

CONCLUSIONS

Previous studies attempting to model SMO rhyolite genesis have largely relied on the whole-rock geochemical and isotopic signatures of volcanic rocks from the northern SMO with constraints on potential lower crustal source regions or assimilants provided by xenolith suites restricted to a few Neogene–Quaternary basaltic volcanic rocks along the eastern margin of the SMO (e.g. Ruiz *et al.*, 1988*a*, 1988*b*; Rudnick & Cameron, 1991; Wark, 1991; Cameron *et al.*, 1992; Smith *et al.*, 1996). The U–Pb zircon age data presented here give the first direct information on crustal materials contributing to SMO rhyolite generation. An advantage of the ELA-ICP-MS technique is the ability to date and chemically analyse a large number of zircons, increasing the opportunity to detect the presence of an inherited component. An important implication of our data is that the age (and hence compositional and isotopic) range of crustal materials involved in SMO rhyolite genesis is greater than previously considered. In addition to the involvement of Proterozoic crustal materials, the presence of Mesozoic to Eocene age zircon indicates inheritance from igneous basement generated during preceding subduction-related magmatic activity (Aguirre-Díaz & McDowell, 1991; Jones *et al.*, 1995; Ferrari *et al.*, 2007). The ages of the xenocrystic and antecrystic zircons suggest that remelting of young crustal materials may have been important in producing the geochemical and isotopic signatures of the SMO rhyolites. The involvement of young, non-radiogenic mafic to intermediate calc-alkaline crust has been considered fundamental in the generation of other large-volume silicic igneous provinces (e.g. Whitsunday and Chon Aike SLIPs, Ewart *et al.*, 1992; Pankhurst & Rapela, 1995; Riley *et al.*, 2001; Bryan *et al.*, 2002). Most recently, the ages of inherited zircons in Taupo Volcanic Zone rhyolites (Brown & Smith, 2004; Charlier *et al.*, 2004) have been used to suggest that melting of Early Cretaceous volcanogenic sedimentary rock may have significantly contributed to rhyolite generation. These volcanogenic sedimentary rocks, regionally extensive in eastern Gondwanaland during the Early Cretaceous, were themselves sourced from coeval, isotopically primitive, calc-alkaline intermediate to silicic explosive volcanism (Bryan *et al.*, 1997; Wandres *et al.*, 2004).

In conclusion, the zircon inheritance age data indicate that end-member models of magma mixing–AFC processes for SMO rhyolite petrogenesis are oversimplified, and that contributions from multiple crustal sources of different ages (Proterozoic, Mesozoic, Tertiary), and chemical and isotopic composition are likely to have been involved. Contributions of crustal materials changed during the lifespan of SMO volcanism as follows: (1) the proportion of igneous underplate and intrusions residing within the crust increased with time; and (2) the locus of mafic magma intrusion and consequent crustal melting migrated laterally and vertically through the crust. The indications of Eocene to Mesozoic age crustal involvement in the oldest SMO rhyolites suggest that at the time when SMO magmatism was initiated, the age of the lower crust may have been significantly younger than the age of exposed basement and different from that sampled by xenoliths in Neogene–Quaternary basaltic lavas. The long-term temporal trend towards a greater contribution of antecrystic SMO-age zircon to the age spectra suggests that continued heat and material fluxes of mantle-derived magmas into the Mexican crust resulted in remelting of igneous rock formed during earlier phases of SMO magmatism, and potentially at upper crustal levels. This may be a common process in regions of long-lived and/or large-volume magmatism (e.g. Large Igneous Provinces) where high-rate and continuing basaltic magma influxes begin remelting earlier-formed igneous underplate and other intrusions residing in the crust.

SUPPLEMENTARY DATA

Supplementary data for this paper are available at *Journal of Petrology* online.

ACKNOWLEDGEMENTS

REFERENCES

Aguirre-Díaz, G. J. & Labarthe-Hernandez, G. (2003). Fissure ignimbrites; fissure-source origin for voluminous ignimbrites of the Sierra Madre Occidental and its relationship with basin and range faulting. *Geology* **31**, 773–776.

Aguirre-Díaz, G. J. & McDowell, F. W. (1991). The volcanic section at Nazas, Durango, Mexico, and the possibility of widespread Eocene volcanism within the Sierra Madre Occidental. *Journal of Geophysical Research* **96**, 13373–13388.

Aguirre-Díaz, G. J., Dubois, M., Laureyns, J. & Schaaf, P. (2002). Nature and *P–T* conditions of the crust beneath the central Mexican Volcanic Belt based on a Precambrian crustal xenolith. *International Geology Review* **44**, 222–242.

Albrecht, A. & Goldstein, S. L. (2000). Effects of basement composition and age on silicic magmas across an accreted terrane–Precambrian crust boundary, Sierra Madre Occidental, Mexico. *Journal of South American Earth Sciences* **13**, 255–273.

Allen, C. M. & Barnes, C. G. (2006). Ages and some cryptic sources of Mesozoic plutonic rocks in the Klamath Mountains, California and Oregon. In: Snoke, A. W. & Barnes, C. G. (eds) *Geological Studies in the Klamath Mountains Province, California and Oregon: A Volume in Honor of William P. Irwin. Geological Society of America, Special Papers* **410**, 223–245.

Anderson, T. H. & Silver, L. T. (1979). The role of the Mojave–Sonora megashear in the tectonic evolution of northern Sonora. In: Anderson, T. H. & Roldán-Quintana, J. (eds) *Geology of Northern Sonora: Guidebook—Field Trip 27.* Annual Meeting of the Geological Society of America, Universidad Nacional Autónoma de México, Instituto de Geología and the University of Pittsburgh, Pittsburgh, pp. 59–68.

Annen, C. & Sparks, R. S. J. (2002). Effects of repetitive emplacement of basaltic intrusions on thermal evolution and melt generation in the crust. *Earth and Planetary Science Letters* **203**, 937–955.

Bachmann, O. & Bergantz, G. W. (2003). Rejuvenation of the Fish Canyon magma body: A window into the evolution of large-volume silicic magma systems. *Geology* **31**, 789–792.

Bachmann, O., Dungan, M. A. & Lipman, P. W. (2002). The Fish Canyon magma body, San Juan volcanic field, Colorado; rejuvenation and eruption of an upper-crustal batholith. *Journal of Petrology* **43**, 1469–1503.

Bachmann, O., Oberli, F., Dungan, M. A., Meier, M., Mundil, R. & Fischer, H. (2007). $^{40}Ar/^{39}Ar$ and U–Pb dating of the Fish Canyon magmatic system, San Juan Volcanic field, Colorado: Evidence for an extended crystallization history. *Chemical Geology* **236**, 134–166.

Bacon, C. R. & Hirschmann, M. M. (1988). Mg/Mn partitioning as a test for equilibrium between coexisting Fe–Ti oxides. *American Mineralogist* **73**, 57–61.

Bacon, C. & Lowenstern, J. B. (2005). Late Pleistocene granodiorite source for recycled zircon and phenocrysts in rhyodacite lava at Crater Lake, Oregon. *Earth and Planetary Science Letters* **233**, 277–293.

Bain, J. H. C. & Draper, J. J. (eds) (1997). North Queensland Geology. *Queensland Geology* **9**, 600 pp.

Ballard, J. R., Palin, J. M., Williams, I. S. & Campbell, I. H. (2001). Two ages of porphyry intrusion resolved for the super-giant Chuquicamata copper deposit of northern Chile be ELA-ICP-MS and SHRIMP. *Geology* **29**, 383–386.

Barboza, S. A. & Bergantz, G. W. (1998). Rheological transitions and the progress of melting crustal rocks. *Earth and Planetary Science Letters* **158**, 19–29.

Bartolini, C. (1998). Stratigraphy, geochronology, geochemistry and tectonic setting of the Mesozoic Nazas formation, North–central Mexico. PhD dissertation, University of Texas, El Paso, 495 pp.

Belousova, E. A., Griffin, W. L., O'Reilly, S. Y. & Fisher, N. I. (2002). Igneous zircon: trace element composition as an indicator of source rock type. *Contributions to Mineralogy and Petrology* **143**, 602–622.

Bence, A. E. & Albee, A. L. (1968). Empirical correction factors for the electron microanalysis of silicate and oxides. *Journal of Geology* **76**, 382–403.

Bergantz, G. W. (1989). Underplating and partial melting implications for melt generation and extraction. *Science* **254**, 1093–1095.

Best, M. G. & Christiansen, E. H. (1991). Limited extension during peak Tertiary volcanism, Great Basin of Nevada and Utah. *Journal of Geophysical Research* **96**, 13509–13528.

Bindeman, I. N., Valley, J. W., Wooden, J. L. & Persing, H. M. (2001). Post-caldera volcanism: *in situ* measurement of U–Pb age and oxygen isotope ratio in Pleistocene zircons from Yellowstone caldera. *Earth and Planetary Science Letters* **189**, 197–206.

Black, L. P., Kamo, S. L., Allen, C. M., Davis, D. W., Aleinikoff, J. N., Valley, J. W., Mundil, R., Campbell, I. H., Korsch, R. J., Williams, I. S. & Foudoulis, C. (2004). Improved $^{206}Pb/^{238}U$ microprobe geochronology by the monitoring of a trace-element-related matrix effect; SHRIMP, ID-TIMS, ELA-ICP-MS and oxygen isotope documentation for a series of zircon standards. *Chemical Geology* **205**, 115–140.

Blount, J. G. (1993). The geochemistry, petrogenesis, and geochronology of the Precambrian meta-igneous rocks of Sierra del Cuervo and Cerro El Carrizalillo, Chihuahua, Mexico. PhD thesis, University of Texas at Austin, Austin, 242 pp.

Blount, J. G., Walker, N. W. & Carlson, W. D. (1988). Geochemistry and U–Pb ages of mid-Proterozoic metaigneous rocks from

Chihuahua, Mexico. *Geological Society of America, Abstracts with Programs* **20**(7), pA205.

Bonner, J. L. & Herrin, E. T. (1999). Surface wave study of the Sierra Madre Occidental of northern Mexico. *Bulletin of the Seismological Society of America* **89**, 1323–1337.

Brown, S. J. A. & Fletcher, I. R. (1999). SHRIMP U–Pb dating of the preeruption growth history of zircons from the 340 ka Whakamaru Ignimbrite, New Zealand; evidence for >250 k.y. magma residence times. *Geology* **27**, 1035–1038.

Brown, S. J. A. & Smith, R. T. (2004). Crystallisation history and crustal inheritance in a large silicic magma system: $^{206}Pb/^{238}U$ ion probe dating of zircons from the 1·2 Ma Ongatiti ignimbrite, Taupo Volcanic Zone. *Journal of Volcanology and Geothermal Research* **135**, 247–257.

Bryan, S. E. (2007). Silicic Large Igneous Provinces. *Episodes* **30**, 20–31.

Bryan, S. E. & Ernst, R. E. (2007). Revised definition of Large Igneous Provinces (LIPs). *Earth-Science Reviews*, doi:10.1016/j.earscirev.2007.08.008.

Bryan, S. E., Constantine, A. E., Stephens, C. J., Ewart, A., Schön, R. W. & Parianos, J. (1997). Early Cretaceous volcano-sedimentary successions along the eastern Australian continental margin: implications for the break-up of eastern Gondwana. *Earth and Planetary Science Letters* **153**, 85–102.

Bryan, S. E., Ewart, A., Stephens, C. J., Parianos, J. & Downes, P. J. (2000). The Whitsunday Volcanic Province, central Queensland, Australia: Lithological and stratigraphic investigations of a silicic-dominated large igneous province. *Journal of Volcanology and Geothermal Research* **99**, 55–78.

Bryan, S. E., Riley, T. R., Jerram, D. A., Leat, P. T. & Stephens, C. J. (2002). Silicic volcanism: an under-valued component of large igneous provinces and volcanic rifted margins. In: Menzies, M. A., Klemperer, S. L., Ebinger, C. J. & Baker, J. (eds) *Magmatic Rifted Margins. Geological Society of America, Special Papers* **362**, 99–120.

Bryan, S. E., Holcombe, R. J. & Fielding, C. R. (2003). Reply to: 'The Yarrol terrane of the northern New England Fold Belt: Forearc or backarc?' Discussion by Murray, C. G., Blake, P. R., Hutton, L. J., Withnall, I. W., Hayward, M. A., Simpson, G. A. & Fordham, B. G. *Australian Journal of Earth Sciences* **50**, 271–293.

Bryan, S. E., Allen, C. M., Holcombe, R. J. & Fielding, C. R. (2004). U/Pb zircon geochronology of Late Devonian to Early Carboniferous extension-related silicic volcanism in the northern New England Fold Belt. *Australian Journal of Earth Sciences* **51**, 645–664.

Busby, C., Smith, D., Morris, W. & Fackler-Adams, B. (1998). Evolutionary model for convergent margins facing large ocean basins: Mesozoic Baja California, Mexico. *Geology* **26**, 227–230.

Busby-Spera, C. J. (1998). Speculative tectonic model for the lower Mesozoic arc of the southwest Cordillera. *Geology* **16**, 1121–1125.

Cameron, K. L. & Cameron, M. (1985). Rare earth element, $^{87}Sr/^{86}Sr$, and $^{143}Nd/^{144}Nd$ compositions of Cenozoic orogenic dacites from Baja California, northwestern Mexico, and adjacent West Texas; evidence for the predominance of a subcrustal component. *Contributions to Mineralogy and Petrology* **91**, 1–11.

Cameron, K. L. & Hanson, G. N. (1982). Rare earth element evidence concerning the origin of voluminous mid-Tertiary rhyolitic ignimbrites and related volcanic rocks, SMO, Chihuahua, Mexico. *Geochimica et Cosmochimica Acta* **46**, 1489–1503.

Cameron, K. L. & Robinson, J. V. (1990). Comments on 'Nd–Sr isotopic compositions of lower crustal xenoliths; evidence for the origin of mid-Tertiary felsic volcanics in Mexico,' by Ruiz J., Patchett P. J. & Arculus R. J. *Contributions to Mineralogy and Petrology* **104**, 609–618.

Cameron, M., Bagby, W. C. & Cameron, K. L. (1980a). Petrogenesis of voluminous mid-Tertiary ignimbrites of the Sierra Madre Occidental. *Contributions to Mineralogy and Petrology* **74**, 271–84.

Cameron, K. L., Cameron, M., Bagby, W. C., Moll, E. J. & Drake, R. E. (1980b). Petrologic characteristics of mid-Tertiary volcanic suites, Chihuahua. *Geology* **8**, 87–91.

Cameron, K. L., Nimz, G. J., Kuentz, D., Niemeyer, S. & Gunn, S. (1989). Southern Cordilleran basaltic andesite suite, southern Chihuahua, Mexico; a link between Tertiary continental arc and flood basalt magmatism in North America. *Journal of Geophysical Research* **94**, 7817–7840.

Cameron, K. L., Robinson, J. V., Niemeyer, S., Nimz, G. J., Kuentz, D. C., Harmon, R. S., Bohlen, S. R. & Collerson, K. D. (1992). Contrasting styles of Pre-Cenozoic and mid-Tertiary crustal evolution in northern Mexico: evidence from deep crustal xenoliths from La Olivina. *Journal of Geophysical Research* **97**, 17353–17376.

Campa, M. F. & Coney, P. J. (1983). Tectono-stratigraphic terranes and mineral resource distributions in Mexico. *Canadian Journal of Earth Sciences* **20**, 1040–1051.

Centeno-García, E., Guerrero-Suastegui, M. & Talavera-Mendoza, O. (2007). The Guerrero Composite Terrane of western Mexico: collision and subsequent rifting in a suprasubduction zone. *Geological Society of America, Special Papers* (in press).

Chappell, B. W., White, A J. R., Williams, I. S., Wyborn, D. & Wyborn, L. A. I. (2000). Lachlan Fold Belt granites revisited: high- and low-temperature granites and their implications. *Australian Journal of Earth Sciences* **47**, 123–138.

Charlier, B. L. A., Wilson, C. J. N., Lowenstern, J. B., Blake, S., Van Calsteren, P. W. & Davidson, J. P. (2004). Magma generation at a large, hyperactive silicic volcano (Taupo, New Zealand) revealed by U–Th and U–Pb systematics in zircons. *Journal of Petrology* **46**, 3–32.

Cleverly, R. W., Betton, P. J. & Bristow, J. W. (1984). Geochemistry and petrogenesis of the Lebombo rhyolites. In: Erlank, A. J. (ed) *Petrogenesis of the Volcanic Rocks of the Karoo Province. Geological Society of South Africa, Special Publication* **13**, 171–195.

Cole, J. W. (1990). Structural control and origin of volcanism in the Taupo Volcanic Zone, New Zealand. *Bulletin of Volcanology* **52**, 445–459.

Coney, P. J. & Campa, M. F. (1987). Lithotectonic terrane map of Mexico (west of the 91st meridian). *US Geological Survey, Miscellaneous Field Studies Map* **MF-1874-D**, scale 1:2 500 000.

Couch, R. W., Ness, G. E., Sanchez-Zamora O., Calderon-Riveroll, G., Doguin, P., Plawman, T., Coperude, S., Huehn, B. & Gumma, W. (1991). Gravity anomalies and crustal structure of the Gulf and Peninsular Province of the Californias. In: Dauphin, J. P. & Simoneit, B. R. T. (eds) *The Gulf and the Peninsular Province of the Californias. American Association of Petroleum Geologists, Memoirs* **47**, 47–70.

Cumming, G. L. & Richards, J. R. (1975). Ore lead isotope ratios in a continuously changing Earth. *Earth and Planetary Science Letters* **28**, 155–171.

Damon, P. E., Shafiqullah, M. & Clark, K. F. (1981). Age trends of igneous activity in relation to metallogenesis in the southern Cordillera. *Arizona Geological Society Digest* **14**, 137–154.

Damon, P. E., Shafiqullah, M. & Clark, K. (1983). Geochronology of the porphyry copper deposits and related mineralization in Mexico. *Canadian Journal of Earth Sciences* **20**, 1052–1071.

De Silva, S. L. (1989a). Altiplano–Puna volcanic complex of the central Andes. *Geology* **17**, 1102–1106.

De Silva, S. L. (1989b). Geochronology and stratigraphy of the ignimbrites from the 21°30'S to 23°30'S portion of the central

Andes of northern Chile. *Journal of Volcanology and Geothermal Research* **37**, 93–131.

Dickinson, W. R. & Lawton, T. F. (2001). Carboniferous to Cretaceous assembly and fragmentation of Mexico. *Geological Society of America Bulletin* **113**, 1142–1160.

Dufek, J. & Bergantz, G. W. (2005). Lower crustal magma genesis and preservation: a stochastic framework for the evaluation of basalt–crust interaction. *Journal of Petrology* **46**, 2167–2195.

Eggins, S. M. & Shelley, J. M. G. (2002). Compositional heterogeneity in NIST SRM 610–617 glasses. *Geostandards Newsletter* **26**, 269–286.

Elías-Herrera, M. & Ortega-Gutiérrez, F. (1997). Petrology of high-grade metapelitic xenoliths in an Oligocene rhyodacite plug—Precambrian crust beneath the southern Guerrero terrane, Mexico? *Revista Mexicana de Ciencias Geológicas* **14**(1), 101–109.

Ewart, A., Schön, R. W. & Chappell, B. W. (1992). The Cretaceous volcanic–plutonic province of the central Queensland (Australia) coast—a rift related 'calc-alkaline' province. *Transactions of the Royal Society of Edinburgh, Earth Sciences* **83**, 327–345.

Ewart, A., Milner, S. C., Armstrong, R. A. & Duncan, A. R. (1998). Etendeka volcanism of the Goboboseb Mountains and Messum Igneous Complex, Namibia. Part II: Voluminous quartz latite volcanism of the Awahab magma system. *Journal of Petrology* **39**, 227–253.

Farmer, G. L. (1992). Magmas as tracers of lower crustal composition: an isotopic approach. In: Fountain, D. M., Arculus, R. & Kay, R. W. (eds) *Continental Lower Crust. Developments in Geotectonics* **23**, 363–390.

Ferrari, L., Lopez-Martinez, M., Aguirre-Díaz, G. & Carrasco-Nuñez, G. (1999). Space–time patterns of Cenozoic arc volcanism in central Mexico: from the Sierra Madre Occidental to the Mexican Volcanic Belt. *Geology* **27**, 303–306.

Ferrari, L., Pasquaré, G., Venegas, S. & Romero, F. (2000). Geology of the western Mexican Volcanic Belt and adjacent Sierra Madre Occidental and Jalisco block. *Geological Society of America, Special Papers* **334**, 65–84.

Ferrari, L., Lopez-Martinez, M. & Rosas-Elguera, J. (2002). Ignimbrite flare-up and deformation in the southern Sierra Madre Occidental, western Mexico; implications for the late subduction history of the Farallon Plate. *Tectonics* **21**(17), 1–23.

Ferrari, L., Valencia-Moreno, M. & Bryan, S. E. (2007). Magmatism and tectonics of the Sierra Madre Occidental and their relation to the evolution of the western margin of North America. *Geological Society of America, Special Papers* **442**, 1–39.

Fuhrman, M. L. & Lindsley, D. H. (1988). Ternary-feldspar modeling and thermometry. *American Mineralogist* **73**, 201–215.

Gans, P. B. (1997). Large-magnitude Oligo-Miocene extension in southern Sonora: Implications for the tectonic evolution of northwest Mexico. *Tectonics* **16**, 388–408.

Gans, P. B. & Bohrson, W. A. (1997). Suppression of volcanism during rapid extension in the Basin and Range Province, United States. *Science* **279**, 66–68.

Gans, P. B., Mahood, G. A. & Schermer, E. R. (1989). Synextensional magmatism in the Basin and Range Province; a case study from the eastern Great Basin. *Geological Society of America, Special Papers* **233**, 1–53.

Gardner, J. E., Layer, P. W. & Rutherford, M. J. (2002). Phenocrysts versus xenocrysts in the youngest Toba Tuff: Implications for the petrogenesis of 2800 km^3 of magma. *Geology* **30**, 347–350.

Ghiorso, M. S. & Sack, R. O. (1991). Fe–Ti oxide geothermometry: thermodynamic formulation and the estimation of intensive variables in silicic magmas. *Contributions to Mineralogy and Petrology* **108**, 485–510.

Gómez-Tuena, A., La Gatta, A., Langmuir, C. H., Goldstein, S. L., Ortega-Gutiérrez, F. & Carrasco-Núñez, G. (2003). Temporal control of subduction magmatism in the eastern Trans-Mexican Volcanic Belt: mantle sources, slab contributions, and crustal contamination. *Geochemistry, Geophysics, Geosystems* **4**(8doi:10.1029/2003GC000524.

González-León, C. M. (1997). Sequence stratigraphy and paleogeographic setting of the Antimonio Formation (Late Permian–Early Jurassic), Sonora, Mexico. *Revista Mexicana de Ciencias Geológicas* **14**, 136–148.

Graham, I. J., Cole, J. W., Briggs, R. M., Gamble, J. A. & Smith, I. E. M. (1995). Petrology and petrogenesis of volcanic rocks from Taupo Volcanic Zone: a review. *Journal of Volcanology and Geothermal Research* **68**, 59–87.

Grajales-Nishimura, J. M., Terrell, D. J. & Damon, P. E. (1992). Evidencias de la prolongación del arco magmático cordillerano del Triásico Tardío-Jurásico en Chihuahua, Durango y Coahuila. *Boletín de la Asociación Mexicana de Geólogos Petroleros* **XLII**, 1–18.

Harris, A. C., Allen, C. M., Bryan, S. E., Campbell, I. H., Holcombe, R. J. & Palin, M. J. (2004). ELA-ICP-MS U–Pb zircon geochronology of regional volcanism hosting the Bajo de la Alumbrera Cu–Au deposit: implications for porphyry-related mineralization. *Mineralium Deposita* **39**, 46–67.

Henry, C. D., McDowell, F. W. & Silver, L. T. (2003). Geology and geochronology of the granitic batholithic complex, Sinaloa, México: Implications for Cordilleran magmatism and tectonics. In: Johnson, S. E., Paterson, S. R., Fletcher, J. M., Girty, G. H., Kimbrough, D. L. & Martin-Barajas, A. (eds) *Tectonic Evolution of Northwestern Mexico and the Southwestern United States. Geological Society of America, Special Papers* **374**, 237–274.

Hess, K.-U. & Dingwell, D. B. (1996). Viscosities of hydrous leucogranitic melts: A non-Arrhenian model. *American Mineralogist* **81**, 1297–1300.

Hildreth, W. (1981). Gradients in silicic magma chambers: implications for lithospheric magmatism. *Journal of Geophysical Research* **86**, 10153–10192.

Hildreth, W. (2001). A critical overview of silicic magmatism. *Penrose Conference on Longevity and Dynamics of Rhyolitic Magma Systems*, Mammoth, CA, 6–12 June 2001.

Hildreth, W. & Moorbath, S. (1988). Crustal contributions to arc magmatism in the Andes of central Chile. *Contributions to Mineralogy and Petrology* **98**, 455–489.

Hoskin, P. W. O. (2005). Trace-element composition of hydrothermal zircon and the alteration of Hadean zircon from the Jack Hills, Australia. *Geochimica et Cosmochimica Acta* **69**, 637–648.

Houghton, B. F., Wilson, C. J. N., McWilliams, M. O., Lanphere, M. A., Weaver, S. D., Briggs, R. M. & Pringle, M. S. (1995). Chronology and dynamics of a large silicic magmatic system: Central Taupo Volcanic Zone, New Zealand. *Geology* **23**, 13–16.

Housh, T. B. & McDowell, F. W. (2007). Isotope provinces in Laramide and mid-Tertiary igneous rocks of northwestern Mexico (Chihuahua and Sonora) and their relation to basement configuration. In: Anderson, T. H., Nourse, A. J., McKee, J. W. & Steiner, B. M. (eds) *The Mojave-Sonora Megashear Hypothesis: Development, Assessment, and Alternatives. Geological Society of America, Special Papers* **393**, 671–692.

Humphreys, E. D., Hessler, E., Dueker, K., Erslev, E., Farmer, G. L. & Atwater, T. (2003). How Laramide-age hydration of North America by the Farallon slab controlled subsequent activity in the western U. S. *International Geology Review* **45**, 575–595.

Huppert, H. E. & Sparks, R. S. J. (1988). The generation of granitic magmas by intrusion of basalt into continental crust. *Journal of Petrology* **29**, 599–642.

James, E. W. & Henry, C. D. (1993). Pb isotopes of ore deposits in Trans-Pecos Texas and northeastern Chihuahua, Mexico: Basement, igneous, and sedimentary sources of metals. *Economic Geology* **88**, 934–947.

Johnson, C. M. (1991). Large-scale crust formation and lithosphere modification beneath Middle to Late Cenozoic calderas and volcanic fields, western North America. *Journal of Geophysical Research* **96**, 13845–13507.

Jones, N. W., McKee, J. W., Anderson, T. H. & Silver, L. T. (1995). Jurassic volcanic rocks in northeastern Mexico: a possible remnant of a Cordilleran magmatic arc. In: Jacques-Ayala, C., Gonzáles-León, C. M. & Roldán-Quintana, J. (eds) *Studies on the Mesozoic of Sonora and Adjacent Areas. Geological Society of America Special Paper* **301**, 179–189.

Keller, P. C. (1977). Geology of the Sierra del Gallego area, Chihuahua, Mexico. PhD thesis, University of Texas at Austin, Austin, 124 pp.

Keller, P. C., Bockoven, N. T. & McDowell, F. W. (1982). Tertiary volcanic history of the Sierra del Gallego area, Chihuahua, Mexico. *Geological Society of America Bulletin* **93**, 303–314.

Klemperer, S. L. (1989). Deep seismic reflection profiling and the growth of the continental crust. *Tectonophysics* **161**, 233–244.

Lanphere, M. A., Cameron, K. L. & Cameron, M. (1980). Sr isotopic geochemistry of voluminous rhyolitic ignimbrites and related rocks, Batopilas area, western Mexico. *Nature* **286**, 594–596.

Levresse, G., González-Partida, E., Carrillo-Chávez, A., Tritlla, J., Camprubi, A., Cheilletz, A., Gasquet, D. & Deloule, E. (2004). Petrology, U/Pb dating and (C–O) stable isotope constraints on the source and evolution of the adakite-related Mezcala Fe–Au skarn district, Guerrero, Mexico. *Mineralium Deposita* **39**, 301–312.

Lightfoot, P. C., Hawkesworth, C. J. & Sethna, S. F. (1987). Petrogenesis of rhyolites and trachytes from the Deccan Trap: Sr, Nd and Pb isotope and trace element evidence. *Contributions to Mineralogy and Petrology* **95**, 44–54.

Lipman, P. W., Prostka, H. J. & Christiansen, R. L. (1972). Cenozoic volcanism and plate-tectonic evolution of the western United States, Part 1: Early and Middle Cenozoic. *Philosophical Transactions of the Royal Society of London Series A* **271**, 217–248.

Lozano-Santa Cruz, R., Verma, S. P., Girón, P., Velasco-Tapia, F., Morán-Zenteno, D., Viera, F. & Chávez, G. (1995). Calibración preliminar de fluorescencia de rayos X para análisis cuantitativo de elementos mayores en rocas ígneas. *Actas INAGEQ* **39**, 203–208.

Ludwig, K. R. (2002). *Isoplot Version 3.00: a Geochronological Tool-kit for Microsoft Excel. Berkeley Geochronology Center, Special Publications.*

Luhr, J. F., Carmichael, I. S. E. & Varecamp, J. C. (1984). The 1982 eruptions of El Chichón volcano, Chiapas, Mexico: mineralogy and petrology of the anhydrite-bearing pumices. *Journal of Volcanology and Geothermal Research* **23**, 69–108.

Lyons, J. I. (1988). Volcanogenic iron oxide deposits, Cerro de Mercado and vicinity, Durango. *Economic Geology* **83**, 1886–1906.

McCulloch, M. T., Kyser, T. K., Woodhead, J. D. & Kinsley, L. (1994). Pb–Sr–Nd–O isotopic constraints on the origin of rhyolites from the Taupo Volcanic Zone of New Zealand: evidence for assimilation followed by fractionation from basalt. *Contributions to Mineralogy and Petrology* **115**, 303–312.

McDowell, F. W. & Clabaugh, S. E. (1979). Ignimbrites of the Sierra Madre Occidental and their relation to the tectonic history of western Mexico. In: Chapin, C. E. & Elston, W. E. (eds) *Ash-flow tuffs. Geological Society of America, Special Papers* **180**, 113–124.

McDowell, F. W. & Keizer, R. P. (1977). Timing of mid-Tertiary volcanism in the Sierra Madre Occidental between Durango City and Mazatlán, Mexico. *Geological Society of America Bulletin* **88**, 1479–1487.

McDowell, F. W. & Mauger, R. L. (1994). K–Ar and U–Pb zircon chronology of Late Cretaceous and Tertiary magmatism in central Chihuahua State, Mexico. *Geological Society of America Bulletin* **106**, 118–132.

McDowell, F. W. & McIntosh, W. C. (2007). Timing of intense magmatic episodes in the northern Sierra Madre Occidental, Mexico. *Geological Society of America, Abstracts with Programs* (in press).

McDowell, F. W., Wark, D. A. & Aguirre-Díaz, G. (1990). The Tertiary ignimbrite flare-up in western Mexico. *Geological Society of America, Abstracts with Programs* **22**, 66.

McDowell, F. W., Housh, T. B. & Wark, D. A. (1999). Nature of crust beneath west–central Chihuahua, Mexico, based upon Sr, Nd, and Pb isotopic compositions at the Tomóchic volcanic center. *Geological Society of America Bulletin* **111**, 823–830.

McDowell, F. W., Roldán-Quintana, J. & Connelly, J. (2001). Duration of Late Cretaceous–early Tertiary magmatism in east–central Sonora, Mexico. *Geological Society of America Bulletin* **113**, 521–531.

Mauger, R. L. (1981). Geology and petrology of the Calera-del Nido block, Chihuahua Mexico. In: Goodell, P. C. (ed.) *Uranium in Volcanic and Volcaniclastic Rocks. American Association of Petroleum Geologists, Studies in Geology* **13**, pp. 202–242.

Mauger, R. L. (1983). Geologic map of the Majalca–Punta de Agua area, central Chihuahua, Mexico. In: Clark, K. F. & Goodell, P. C. (eds) *Geology and Mineral Resources of North-central Chihuahua. Guidebook of the El Paso Geological Society Field Conference*, pp. 169–174.

Maughan, L. L., Christiansen, E. H., Best, M. G., Sherman Grommé, C., Deino, A. L. & Tingey, D. G. (2002). The Oligocene Lund Tuff, Great Basin, USA: a very large volume monotonous intermediate. *Journal of Volcanology and Geothermal Research* **113**, 129–157.

Miller, J. S. & Wooden, J. L. (2004). Residence, resorption and recycling of zircons in Devils Kitchen Rhyolite, Coso Volcanic Field, California. *Journal of Petrology* **45**, 2155–2170.

Miller, C. F., Meschter McDowell, S. & Mapes, R. W. (2003). Hot and cold granites? Implications of zircon saturation temperatures and preservation of inheritance. *Geology* **31**, 529–532.

Mori, L., Gomez-Tuena, A., Cai, Y. & Goldstein, S. L. (2007). Effects of prolonged flat subduction on the Miocene magmatic record of the central Trans-Mexican Volcanic Belt. *Chemical Geology* **244**, 452–473.

Nieto-Samaniego, Á. F., Ferrari, L., Alaniz-Alvarez, S. A., Labarthe-Hernández, G. & Rosas-Elguera, J. (1999). Variation of Cenozoic extension and volcanism across the southern Sierra Madre Occidental volcanic province, Mexico. *Geological Society of America Bulletin* **111**, 347–363.

Ortega-Gutiérrez, F., Sedlock, R. L. & Speed, R. C. (1994). Phanerozoic tectonic evolution of Mexico. In: Speed, R. C. (ed.) *Phanerozoic Evolution of North American Continent–Ocean Transitions. Geological Society of America, Decade of North American Geology Summary Volume to Accompany the DNAG Continent–Ocean Transects Series.* Boulder, CO: Geological Society of America, pp. 265–306.

Pankhurst, R. J. & Rapela, C. R. (1995). Production of Jurassic rhyolite by anatexis of the lower crust of Patagonia. *Earth and Planetary Science Letters* **134**, 25–36.

Pankhurst, R. J., Leat, P. T., Sruoga, P., Rapela, C. W., Márquez, M., Storey, B. C. & Riley, T. R. (1998). The Chon Aike silicic igneous province of Patagonia and related rocks in Antarctica: a silicic large igneous province. *Journal of Volcanology and Geothermal Research* **81**, 113–136.

Pankhurst, R. J., Riley, T. R., Fanning, C. M. & Kelley, S. P. (2000). Episodic silicic volcanism along the proto-Pacific margin of Patagonia and the Antarctic Peninsula: plume and subduction influences associated with the break-up of Gondwana. *Journal of Petrology* **41**, 605–625.

Parson, L. M. & Wright, I. C. (1996). The Lau–Havre–Taupo back-arc basin: a southward- propagating, multi-stage evolution from rifting to spreading. *Tectonophysics* **263**, 1–22.

Patiño Douce, A. E. (2000). What do experiments tell us about the relative contributions of crust and mantle to the origin of granitic magmas? In: Castro, A., Fernandez, C. & Vigneresse, J. L. (eds) *Understanding Granites: Integrating New and Classical Techniques. Geological Society, London, Special Publications* **168**, 55–75.

Perry, F. V., DePaolo, D. J. & Baldridge, W. S. (1993). Neodymium isotopic evidence for decreasing crustal contributions to Cenozoic ignimbrites of the western United States: implications for the thermal evolution of the Cordilleran crust. *Geological Society of America Bulletin* **105**, 872–882.

Reid, M. R., Coath, C. D., Harrison, T. M. & McKeegan, K. D. (1997). Prolonged residence times for the youngest rhyolites associated with Long Valley caldera: ^{230}Th–^{238}U ion microprobe dating of young zircons. *Earth and Planetary Science Letters* **150**, 27–39.

Riley, T. R., Leat, P. T., Pankhurst, R. J. & Harris, C. (2001). Origins of large volume rhyolitic volcanism in the Antarctic Peninsula and Patagonia by crustal melting. *Journal of Petrology* **42**, 1043–1065.

Rohrlach, B. D. (2002). Tectonic evolution, petrochemistry, geochronology and palaeohydrology of the Tampakan porphyry and high sulphidation epithermal Cu–Au deposit Mindanao, Philippines. PhD thesis, Australian National University, Canberra, 139 pp.

Rubatto, D. & Hermann, J. (2007). Experimental zircon/melt and zircon/garnet trace element partitioning and implications for the geochronology of crustal rocks. *Chemical Geology* **241**, 38–61.

Rudnick, R. L. & Cameron, K. L. (1991). Age diversity of the deep crust in northern Mexico. *Geology* **19**, 1197–1200.

Ruiz, J., Patchett, P. J. & Arculus, R. J. (1988*a*). Nd–Sr isotope composition of lower crustal xenoliths—evidence for the origin of mid-Tertiary felsic volcanics in Mexico. *Contributions to Mineralogy and Petrology* **99**, 36–43.

Ruiz, J., Patchett, P. J. & Ortega, F. (1988*b*). Proterozoic and Phanerozoic basement terranes of Mexico from Nd isotopic studies. *Geological Society of America Bulletin* **100**, 274–281.

Ruiz, J., Patchett, P. J. & Arculus, R. J. (1990). Reply to 'Comments on Nd–Sr isotope composition of lower crustal xenoliths—evidence for the origin of mid-Tertiary felsic volcanics in Mexico' by Cameron, K. L. & Robinson, J. V. *Contributions to Mineralogy and Petrology* **104**, 615–618.

Schaaf, P., Hall, B V. & Bissig, T. (2003). The Puerto Vallarta Batholith and Cuale Mining District, Jalisco, Mexico—high diversity parenthood of continental arc magmas and Kuroko-type volcanogenic massive sulphide deposits. In: *Geologic transects across Cordilleran Mexico, Guidebook for the field trips of the 99th Geological Society of America Cordilleran Section Annual Meeting, Puerto Vallarta, Jalisco, Mexico, 31 March 2003 Mexico, D.F., Universidad Nacional Autónoma de México. Instituto de Geología, Publicación Especial 1, Field Trip 8*, pp. 183–199.

Scheubel, F. R., Clark, K. F. & Porter, E. W. (1988). Geology, tectonic environment, structural controls in the San Martin de Bolaños District, Jalisco. *Economic Geology* **83**, 1703–1720.

Schmitz, M. D. & Bowring, S. A. (2001). U–Pb zircon and titanite systematics of the Fish Canyon Tuff: an assessment of high-precision U–Pb geochronology and its application to young volcanic rocks. *Geochimica et Cosmochimica Acta* **65**, 2571–2587.

Sedlock, R., Ortega-Gutiérrez, F. & Speed, R. C. (1993). *Tectonostratigraphic Terranes and Tectonic Evolution of Mexico. Geological Society of America, Special Papers* **278**, 153 pp.

Simon, J. I. & Reid, M. R. (2005). The pace of rhyolite differentiation and storage in an 'archetypical' silicic magma system, Long Valley, California. *Earth and Planetary Science Letters* **235**, 123–140.

Smith, R. D., Cameron, K. L., McDowell, F. W., Niemeyer, S. & Sampson, D. E. (1996). Generation of voluminous silicic magmas and formation of mid-Cenozoic crust beneath north–central Mexico; evidence from ignimbrites, associated lavas, deep crustal granulites, and mantle pyroxenites. *Contributions to Mineralogy and Petrology* **123**, 375–389.

Solé, J., Salinas Prieto, J. C., Gonzalez Torres, E. & Cendeja Cruz, E. (2007). Edades K–Ar de 54 rocas ígneas y metamórficas del occidente, centro y sur de México. *Revista Mexicana de Ciencias Geológicas* **24**, 104–119.

Stewart, J. H. (1988). Latest Proterozoic and Paleozoic southern margin of North America and the accretion of Mexico. *Geology* **16**, 186–189.

Stewart, J. H. & Roldán-Quintana, J. (1991). Upper Triassic Barranca Group; Nonmarine and shallow-marine rift-basin deposits of northwestern Mexico. In: Pérez-Segura, E. & Jacques-Ayala, C. (eds) *Studies of Sonoran Geology. Geological Society of America, Special Papers* **254**, 19–36.

Swanson, E. R. & McDowell, F. W. (1984). Calderas of the Sierra Madre Occidental volcanic field western Mexico. *Journal of Geophysical Research* **89**, 8787–8799.

Swanson, E. R. & McDowell, F. W. (1985). Geology and geochronology of the Tomochíc caldera, Chihuahua, Mexico. *Geological Society of America Bulletin* **96**, 1477–1482.

Swanson, E. R., Keizer, R. P., Lyons, J. I. & Clabaugh, S. E. (1978). Tertiary volcanism and caldera development near Durango City, Sierra Madre Occidental, Mexico. *Geological Society of America Bulletin* **89**, 1000–1012.

Swanson, E. R., Kempter, K. A., McDowell, F. W. & McIntosh, W. C. (2006). Major ignimbrites and volcanic centers of the Copper Canyon area; a view into the core of Mexico's Sierra Madre Occidental. *Geosphere* **2**, 125–141.

Tamura, Y. & Tatsumi, Y. (2002). Remelting of an andesitic crust as a possible origin for rhyolitic magma in oceanic arcs; an example from the Izu–Bonin Arc. *Journal of Petrology* **43**, 1029–1047.

Torres, R., Ruiz, J. & Patchett, J. (1999). Permo-Triassic continental arc in eastern Mexico: tectonic implications for reconstructions of southern North America. In: Bartolini, C., Wilson, J. L. & Lawton T. F. (eds) *Mesozoic Sedimentary and Tectonic History of North–Central Mexico. Geological Society of America, Special Papers* **340**, 191–196.

Vaggelli, G., Olmi, F. & Conticelli, S. (1999). Quantitative electron microprobe analysis of reference silicate mineral and glass samples. *Acta Vulcanologica* **11**, 297–303.

Valencia-Moreno, M., Ruiz, J. & Roldán-Quintana, J. (1999). Geochemistry of Laramide granitic rocks across the southern margin of the Paleozoic North American continent, Central Sonora, Mexico. *International Geology Review* **41**, 845–857.

Valencia-Moreno, M., Ruiz, J., Barton, M. D., Patchett, P. J., Zürcher, L., Hodkinson, D. & Roldán-Quintana, J. (2001).

A chemical and isotopic study of the Laramide granitic belt of northwestern Mexico: identification of the southern edge of the North American Precambrian basement. *Geological Society of America Bulletin* **113**, 1409–1422.

Valencia-Moreno, M., Ruiz, J., Ochoa-Landín, L., Martínez-Serrano, R. & Vargas-Navarro, P. (2003). Geology and Geochemistry of the Coastal Sonora Batholith, Northwestern Mexico. *Canadian Journal of Earth Sciences* **40**, 819–831.

Vazquez, J. A. & Reid, M. R. (2002). Time scales of magma storage and differentiation of voluminous high-silica rhyolites at Yellowstone caldera, Wyoming. *Contributions to Mineralogy and Petrology* **144**, 274–285.

Verma, S. P., Lozano-Santa Cruz, R., Girón, P. & Velasco-Tapia, F. (1996). Calibración preliminar de fluorescencia de rayos×para análisis cuantitativo de elementos traza en rocas ígneas. *Actas INAGEQ* **2**, 237–242.

Vetere, F., Behrens, H., Holtz, F. & Neuville, D. R. (2006). Viscosity of andesitic melts—new experimental data and a revised calculation model. *Chemical Geology* **228**, 233–245.

Wandres, A. M., Bradshaw, J. D., Weaver, S., Maas, R., Ireland, T. & Eby, N. (2004). Provenance analysis using conglomerate clast lithologies: a case study from the Pahau terrane of New Zealand. *Sedimentary Geology* **167**, 57–89.

Ward, P. L. (1995). Subduction cycles under western North America during the Mesozoic and Cenozoic eras. In: Miller, D. M. & Busby, C. (eds) *Jurassic Magmatism and Tectonics of the North American Cordillera. Geological Society of America, Special Papers* **299**, 1–45.

Wark, D. A. (1991). Oligocene ash flow volcanism, northern Sierra Madre Occidental: Role of mafic and intermediate-composition magmas in rhyolite genesis. *Journal of Geophysical Research* **96**, 13389–13411.

Wark, D. A., Kempter, K. A. & McDowell, F. W. (1990). Evolution of waning, subduction-related magmatism, northern Sierra Madre Occidental, Mexico. *Geological Society of America Bulletin* **102**, 1555–1564.

Watson, E. B. (1996). Dissolution, growth and survival of zircons during crustal fusion: kinetic principles, geological models and implications for isotopic inheritance. *Transactions of the Royal Society of Edinburgh: Earth Sciences* **87**, 43–56.

Watson, E. B. & Harrison, T. M. (1983). Zircon saturation revisited: temperature and composition effects in a variety of crustal magma types. *Earth and Planetary Science Letters* **64**, 295–304.

Wen, S. & Nekvasil, H. (1994). SOLVCALC: An interactive graphics program package for calculating the ternary feldspar solvus and for two-feldspar geothermometry. *Computers and Geosciences* **20**, 1025–1040.

Wilson, C. J. N., Houghton, B. F., McWilliams, M. O., Lanphere, M. A., Weaver, S. D. & Briggs, R. D. (1995). Volcanic and structural evolution of Taupo Volcanic Zone, New Zealand: a review. *Journal of Volcanology and Geothermal Research* **68**, 1–28.

APPENDIX
K/Ar analysis

K/Ar analysis was undertaken at Activation Laboratories Ltd, Canada. The K concentration was determined by ICP, with the sample aliquot weighed into a graphite crucible with lithium metaborate–tetraborate flux and then fused using a LECO induction furnace. The fusion bead was dissolved with acid. All standards, blanks and sample were analysed on a Thermo Jarrell Ash Enviro II ICP Spectrometer. The argon analysis was performed using the isotope dilution procedure on a noble gas mass spectrometer. The sample aliquot was weighed into an Al container, loaded into the sample system of an extraction unit, and degassed at $\sim$100°C over 2 days to remove the surface gases. Argon was extracted from the sample in a double vacuum furnace at 1700°C. Argon concentration was determined using isotope dilution with an ^{38}Ar spike, which is introduced to the sample system prior to each extraction. The extracted gases were cleaned in a two-step purification system. Then pure Ar was introduced into the magnetic sector mass spectrometer (Reinold-type) with a Varian CH5 magnet. The ion source has an axial design (Baur–Signer source), which provides more than 90% transmission and extremely small isotopic mass-discrimination. Measurement of Ar isotope ratios was corrected for mass-discrimination and then atmospheric argon was removed assuming that ^{36}Ar is only from the air. Concentration of ^{40}Ar radiogenic was calculated using the ^{38}Ar spike concentration. After each analysis, the extraction temperature of the furnace was elevated to 1800°C for a few minutes in preparation for the next analysis.

Electron microprobe analysis

Chemical compositions of mineral phases for BOL2 and BOL4 were determined using a JEOL 8600 Superprobe at the CNR-IGG, Earth Science Department, University of Florence. The microprobe is equipped with four spectrometers and operating conditions were 15 kV and 10 nA. Matrix effects were corrected following the Bence & Albee (1968) method. Analytical data on reference samples showed a good precision with a coefficient of variation lower than 3% on major elements, in accordance with estimated precision and accuracy given by Vaggelli *et al.* (1999).

Geochemical analysis

Samples of the BOL2 and BOL4 ignimbrites were first crushed with a steel mill. Ash and pumice fragments were manually separated under a binocular microscope from lithic fragments and the outer parts of chips that were altered. The sample was then crushed manually down to 4 mm and finally crushed using an alumina shatterbox mill.

Major elements were determined by X-ray fluorescence spectroscopy (XRF) using a Siemens SRS-3000 instrument in the Laboratorio Universitario de Geoquíca Isotópica, UNAM, following the procedures of Lozano-Santa Cruz *et al.* (1995) and Verma *et al.* (1996).

Trace element data were obtained by inductively coupled plasma mass spectrometry (ICP-MS) at the Centro de

Geociencias, UNAM, using a Thermo Series XII instrument. Sample preparation was in a clean laboratory environment where ∼50 mg of powdered sample was digested in 1 ml HF plus 0·5 ml 8N HNO_3 in closed screw-top Savillex Teflon beakers, and put on a hot plate overnight at ∼100°C. Acids were evaporated to dryness and further fluxed twice with 15 drops of 16N HNO_3 to break down fluorides. Once the acid was evaporated to dryness, 2 ml deionized water plus 2 ml 8N HNO_3 were added, and the samples were left closed overnight on a hot plate at ∼100°C. All samples were in complete solution after this step. The samples were then diluted to 1:2000 to provide adequate concentrations within the instrument detection limits and to yield the strong signals required for high-precision data. All samples were diluted with an internal standard solution made of Ge (10 ppb), In (5 ppb), Tm (5 ppb) and Bi (5 ppb) to monitor instrumental drift. Calibration and data reduction were based on digestion of international rock standards (AGV-2, BHVO-2, BCR-2, JB-2, JR-1, ZZ), two blanks that followed the same chemical procedure as the samples, and repeated analyses of an in-house basalt standard (sample PS-99-25 from the Palma Sola Massif; Gómez-Tuena *et al.*, 2003). Reproducibility of the trace element data is based on multiple digestions of the international rock standards as reported by Mori *et al.* (2007).